STABILITY OF DOMAINS IN MAGNETIC BUBBLE GARNET FILMS SUBJECTED TO AN IN-PLANE FIELD

by

XINHE CHEN

A thesis
presented to the University of Manitoba
in partial fulfillment of the
requirements for the degree of
M.Sc.
in
DEPARTMENT OF PHYSICS

Winnipeg, Manitoba

Feb.5,1985

STABILITY OF DOMAINS IN MAGNETIC BUBBLE GARNET FILMS SUBJECTED TO AN IN-PLANE FIELD

BY

XINHE CHEN

A thesis submitted to the Faculty of Graduate Studies of the University of Manitoba in partial fulfillment of the requirements of the degree of

MASTER OF SCIENCE

ABSTRACT

The validity of the theories of stripe domain stability were tested when the magnetic field H was applied parallel and perpendicular to the [111] normal of bubble garnet films.

The procedure requires the results of different magnetic measurements, as a function of applied field H, to be consistent with the calculations based on an expression for the energy per unit volume of the stripe lattice. Specially, the procedure is evaluated by a comparison of the magnetically determined thickness to the corresponding optical value.

The experimental input parameters which we used are outlined below. For H parallel to the [111] easy axis experimental values for the sample's initial susceptibility and the stripe collapse field, Hsc, were obtained, using an established AC technique. For H along an in-plane <110> direction the field required to eliminate the domain structure, H^{*}, is obtained. Finally ferromagnetic resonance experiments provided values of $2Ku/Ms-4\pi Ms$ and K_1/Ms; where Ku and K_1 are the uniaxial and cubic anisotropy constants, and Ms is the sample's saturation magnetization. These experimental parameters provide a consistent set of t, $4\pi Ms$, ℓ,

and H_K . Here t is the effective magnetic thickness, ℓ the characteristic length and $H_K = 2Ku/Ms + K_1/Ms$ is the effective anisotropy field.

The results are summarized as follows:

1. In the case when the magnetic field H is applied along the normal of (111) bubble garnet films, the theory of Kooy and Enz * is good enough to describe the stability condition of the stripe domains.
2. When an in-plane magnetic field is applied to (111) films in <110> direction, Druyvesteyn's theory ** is not sufficient to describe the behaviour of the stripe domains in this case. After considering the effects of cubic anisotropy and the demagnetizing energy on the wall energy and the total energy, we found that this modified model gave good agreement between the thickness from two independent measurements.

* C.Kooy and U.Enz,Philips Res. Repts.15,7(1960)

** W.F.Druyvesteyn, J.W.F.Dorleijn and P.J.Rijnierse, J.Appl.Phys.44,2397(1973)

ACKNOWLEDGEMENTS

The author wishes to express his deepest appreciation to Professor C.W. Searle for his constant guidance, counsel and assistance during the course of this investigation. The author is also grateful to Dr. I.Maartense for his constant counsel and assistance in this work and in the preparation of the manuscript.

The financial support in part for this work from Professor C.W.Searle is also appreciated.

At last, the author expresses his appreciation to those who gave,more or less, any kinds of assistance during the study.

NOTATION

A——exchange constant

D——domain period

H_n^*——in-plane field required to eliminate the domain structure

H_k——effective anisotropy field

H_{sc}—stripe collapse field

k——extinction coefficient

K_1——cubic anisotropy constant

K_u——uniaxial anisotropy constant

l——characteristic length

M_s——saturation magnetization

n^*——complex refractive index

t——thickness of the bubble garnet film

$t_{opt.}$—thickness of the bubble garnet film from optical measurement

w——domain stripewidth

σ——domain wall energy

χ_o——initial susceptibility

μ——permeability

CONTENTS

Chapter I

INTRODUCTION

Stripe domains in bubble garnet films with the easy axis of magnetization perpendicular to the film surface have been studied for many years. Kooy and Enz [1] provided a theoretical and experimental account of the behavior of such domains in a field applied perpendicular to the film surface. Druyvesteyn et al. [2] studied the behavior of the domains in an applied in-plane field. Shimada et al [3] had reported their experimental findings on domains in arbitrarily oriented fields,and Yang and Muler [4] provided a theory to account for Shimada's observations. It is the purpose of this work to give a demonstration of a new method which could be used to check the validity of the theories of the stripe domain stability conditions in the two cases when the magnetic field H is applied parallel to the (111) plane or perpendicular to it.

Maartense et al.[5] developed a low frequency susceptibility technique which needs one parameter, either film thickness,t,or domain stripewidth,w, to be measured optically; then, respectively, w or t can be obtained from the initial susceptibility, $\chi|_{M=0}=\chi_0$, and the saturation magnetiza-

tion, $4\pi Ms$, is then deduced from the stripe collapse field Hsc.By making use of the theory of Kooy and Enz [1], and the stability conditions given by Thiele [6],Maartense et al. had shown some graphs which can be used to obtain the relations between the normalized stripe collapse field $Hsc/4\pi Ms$ and the normalized characteristic length ℓ/t. This relation is useful for the present purpose and is plotted in Fig.1.

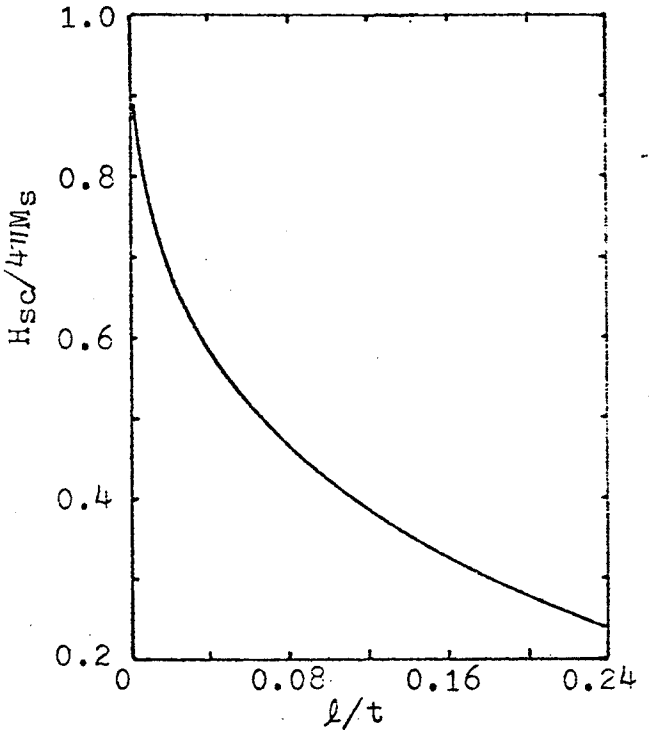

Fig.1 Normalized stripe collapse field versus normalized characteristic length

With the measured value of Hsc and the help of Fig.1, we can plot a line which relates $4\pi Ms$ to ℓ/t for a given Hsc. A typical graph is shown in Fig.2 .

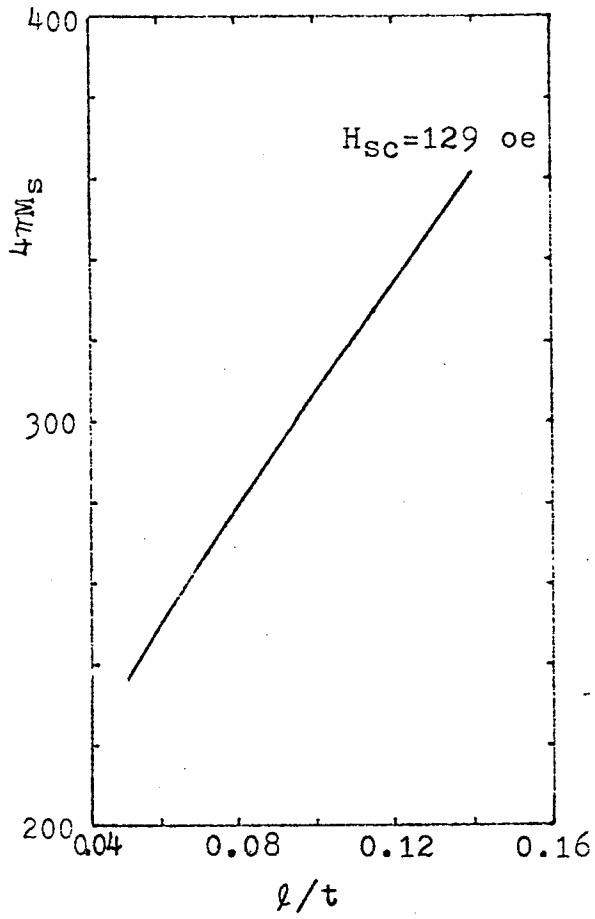

Fig.2 Saturation magnetization versus normalized characteristic length for a given stripe collapse field

Druyvesteyn et al.[2] had studied the stability condition for stripe domains when the magnetic field H was applied in the film plane, see Fig.3 . The method consists of applying a field $H_{\parallel}$ parallel to the plane of the sample, and thus perpendicular to the easy direction of magnetization, and observing the critical field $H_{\parallel}^{*}$ at which the stripe domain pattern disappears. The energy per unit volume of the stripe lattice used in their calculation is

$$E=\frac{2\sigma}{D}+Ku\cos^2\theta_o-MsH_{//}\cos\theta_0+8\pi Ms^2\frac{D\sin^2\theta_0}{t\ \pi^3}\sum_{n=odd}^{\infty}\frac{1}{n^3}[1-\exp(-\frac{2\pi nt}{D})] \qquad (1.1)$$

where Ku is the uniaxial anisotropy constant, D=2w,is the domain period, and σ is the domain wall energy which is expressed as

$$\sigma=4(AKu)^{1/2}\int_0^{\theta_0}[\cos^2\theta-(\frac{MsH_{//}}{Ku})\cos\theta-\cos^2\theta_0+(\frac{MsH_{//}}{Ku})\cos\theta_0]^{1/2}d\theta \qquad (1.2)$$

per unit area,where A is the exchange constant. The expression (1.1) is valid as long as the thickness of the wall is small compared to the width of the stripe domains.

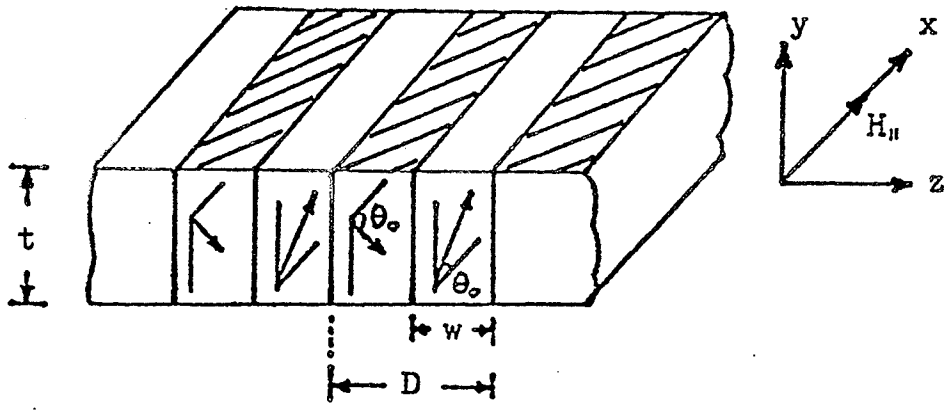

Fig.3 The geometry of the bubble film. The magnetization inside the domains is indicated by arrows.The platelet is infinitely large in the X and Z directions.

By setting the first derivatives of E with respect to θ_0 and D/t to zero, respectively, and using the stability condition of the stripe domains, i.e.,

$$\frac{\partial^2 E}{\partial \theta_0^2}\,\frac{\partial^2 E}{\partial (D/t)^2} - \left(\frac{\partial^2 E}{\partial \theta_0\,\partial (D/t)}\right)^2 = 0 \qquad (1.3)$$

they obtained a plot of $H_{\parallel}^*/H_K$ as a function of $H_{\parallel}^*/4\pi Ms$ (as is shown in Fig.4), where H_K is, according to their definition, 2Ku/Ms.

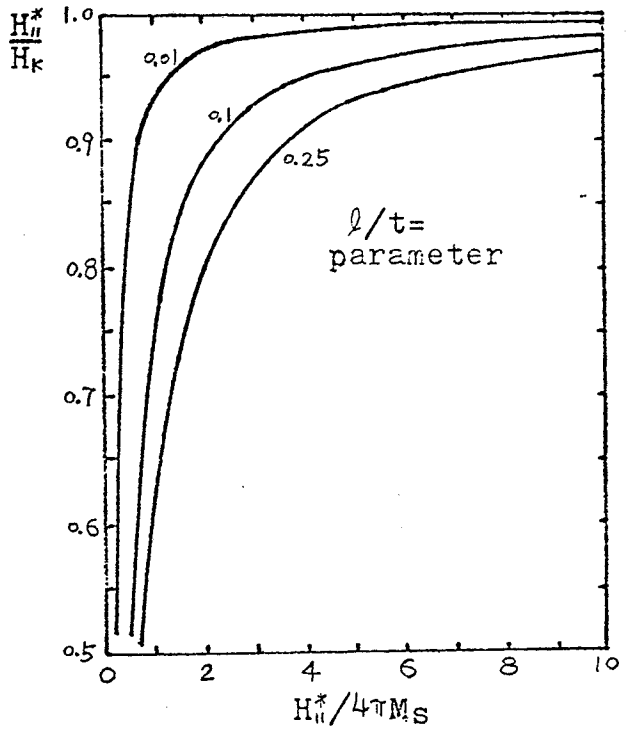

Fig.4 Plot of $H_{\parallel}^*/H_K$ as a function of $H_{\parallel}^*/4\pi Ms$ illustrating the deviation of $H_{\parallel}^*$ from H_K (after Druyvesteyn,et al.,Ref.2)

It is quite easy to see from Fig.4 that $H_{\parallel}^*/4\pi Ms$ has a certain relation with ℓ/t for a given value of $H_{\parallel}^*/H_K$. Since both $H_{\parallel}^*$ and $2Ku/Ms-4\pi Ms$ can be measured experimentally, it

is useful to replot the lines in Fig.4 in another way, i.e., $4\pi Ms$ versus ℓ/t for a given value of $H_f^*/(2Ku/Ms-4\pi Ms)$, as is shown in Fig.5 .

In general, the curves in Fig.2 and Fig.5 are not parallel when they are plotted on the same graph, and they must intersect each other somewhere. This intersection can be used, in principle, to obtain the magnetic thickness and the other static parameters of the bubble garnet films. Then,we can compare the thickness obtained in this way with the optical one of the same sample on the assumption that two values are almost the same for practical bubble films. In this way, we can check the validity of two theories of domain stabilities. In practice, however,it was found that some modification of the energy term in equations (1.1) and (1.2) must be made in order to get reasonable results. The modification will be discussed in Chapter III.

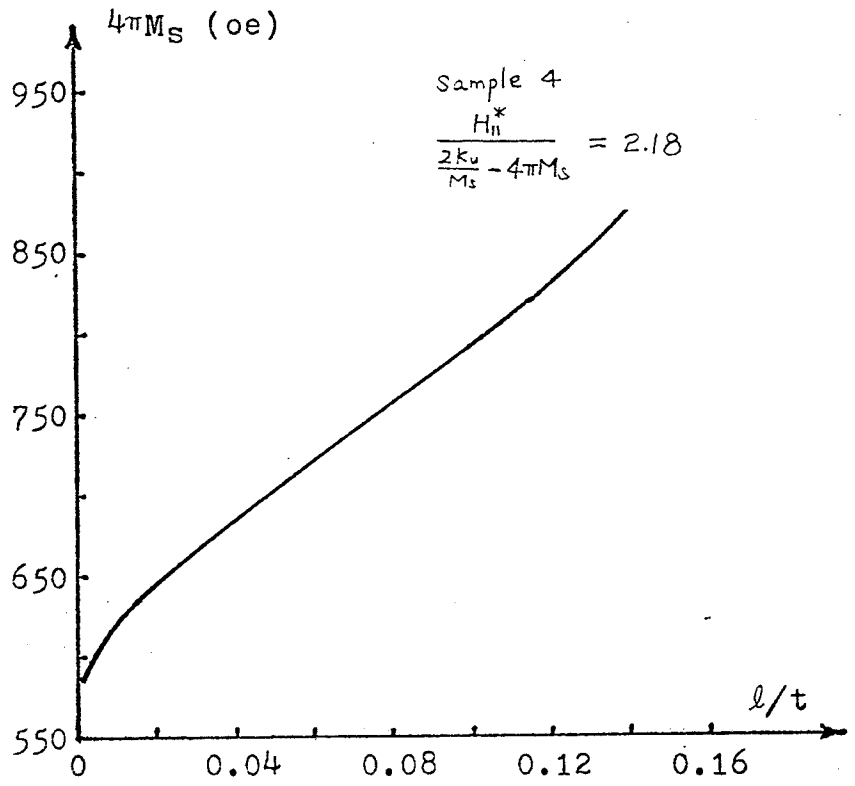

Fig.5 $4\pi M_s$ versus ℓ/t for a given value of $H_{\parallel}^*/(2K_u/M_s - 4\pi M_s)$; the calculation is based on the stability condition of the stripe domains when an in-plane field $H_{\parallel}$ is applied. The energy term is expressed as Eq.(1.1).

Chapter II

EXPERIMENTAL APPARATUS

2.1 MICROWAVE SPECTROMETER

A block diagram of a KU-band microwave spectrometer for a transmission cavity is shown in Fig.6.

A NARDA Model 438 klystron power supply was used to supply the necessary voltages and current to the Varian X-12 Ku-band reflex klystron. A number of microwave devices, such as EH tuners and isolators, were used to optimize the matching of the various components of the spectrometer. The frequency was measured by wave meter. The frequency drifting caused by temperature fluctuations was minimized by putting the klystron into an oil bath which was maintained at a constant temperature by circulating cool water through a copper tube inserted into the oil bath. A frequency stabilizer manufactured by Teltronics was also used to lock the klystron frequency to a reference cavity frequency. In the present experiment, only one cavity was used which functioned as both reference and experimental cavity. The quality factor of the cavity , Q, was estimated as 500-1000,as determined by measuring the frequencies which correspond to the gain of

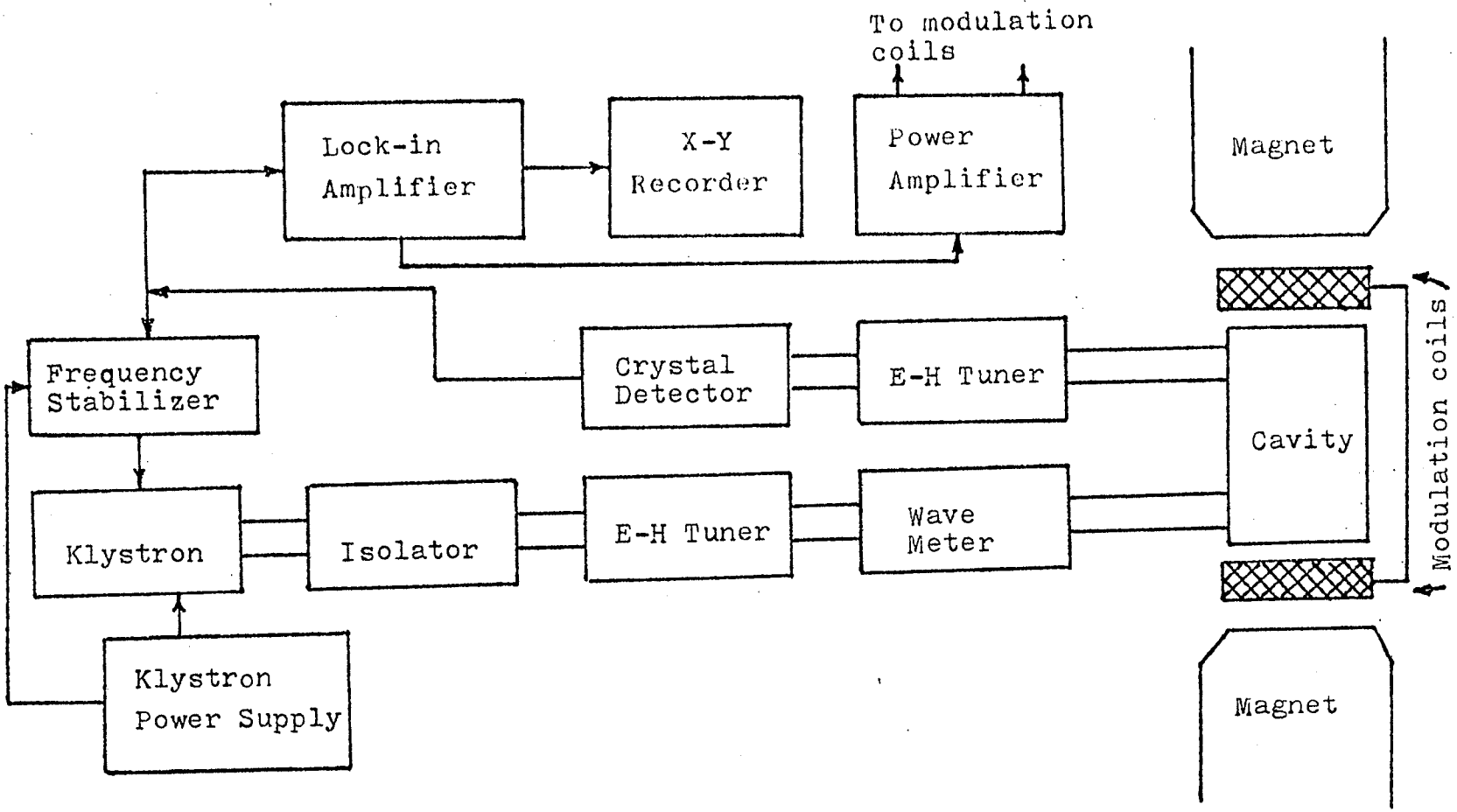

Fig.6 Block diagram of the ferromagnetic spectrometer for a transmission cavity

-3db. The sample was put on the cavity wall during the resonance measurement at a position where the microwave magnetic field was a maximum.

A PAR Model 120 lock-in amplifier was used to amplify the resonance signal from the detector to drive an X-Y recorder. The frequency of the modulation signal produced by the lock-in amplifier was about 1.5 kHz. The modulation signal was fed into the Helmholtz coils after being amplified. The peak value of the modulation field was 10-20 Oe. which was much smaller than the width of the resonance curves. The phase knob was adjusted carefully to maximize the output during the experiment.

The magnetic field was supplied by a Varian Fieldial magnet with a 6.5 cm gap between the poles. Magnetic fields up to 10 kilo-Oersteds could be attained. The magnetic field was read out directly from the dial whose calibration accuracy was about 0.2 % in this range. The control unit also had a sweep function and the sweeping time could be adjusted from 0.5 minutes to 100 minutes, and the sweeping range could be adjusted from 250 milli-Oersteds to 10 kilo-Oersteds. Most frequently, a sweep time of 2.5 minutes and a sweep range of 2.5 kilo-Oersteds were used.

2.2 AC SUSCEPTIBILITY APPARATUS

The AC susceptibility technique was discussed in detail by Maartense[7]. The block diagram of the basic susceptibility apparatus is shown in Fig.7 .

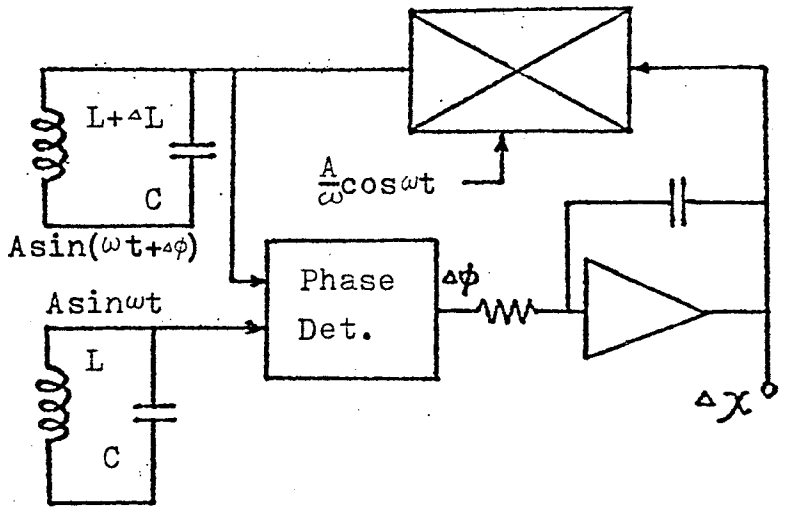

Fig.7 Block diagram of the basic susceptibility apparatus(after Maartense, Ref.7)

Two LC resonators operate at the same frequency ω, which is usually determined by one of the resonators configured as an oscillator. If the presence of a magnetic material causes a differential change ΔL in the self-inductance of the sensor coil L, the resulting phase diffrence $\Delta\phi$ is used as the error signal within a feedback loop which keeps $\Delta\Phi$ nominally at zero. The control element is a multiplier circuit operating as an effective reactance by having as one of its inputs a signal proportional to the integral of the sensor

voltage. The response times of the system are chosen to be about 10 ms when operating with f=10kHz. The sensor field ranges from 1 to 10 Oersteds peak to peak.

The bias coil was driven by a KEPCO bipolar operational power supply which could supply a maximum DC current of about 5 A,which corresponds with the maximum bias field of over 500 Oersteds which would be used to measure the stripe collapse field and the initial susceptibility. The bias field was calibrated by the known stripe field of a sample, and was read on a digital multimeter. The same parameter of each sample was measured at least three times to obtain the average value in order to reduce the fluctuation caused by some sources such as , for example, the fluctuation of the temperature of the coils during the measurement. For the samples with high stripe collapse field, care was taken to avoid the coils' becoming too warm. A material, Gd_2O_3, was used to calibrate the initial susceptibility. The sweep rate of the field was controlled manually.

2.3 SPECTROPHOTOMETER

A CARY recording spectrophotometer Model 14 was used to obtain the optical thickness of the films. The samples were cleaned with acetone to remove possible contamination by grease and then dried in air. The sweeping range was from 0.4 to 2.6 microns in wavelength. There were two light channels, one was the reference channel and the other the

signal channel. The films were measured immediately after the reference was set up by measuring the intensity of the output without anything in either channel, i.e., using air as a reference. The theoretical calculation will be given in Chapter V.

Chapter III

AC SUSCEPTIBILITY AND DOMAIN INSTABILITY

3.1 CRYSTAL ALIGNMENT

With h_{ac}, the sensor field, normal to the film plane and the bias field held at zero, the susceptibility as a function of in-plane field, $H_{//}$, has the same general behavior as is seen with optical techniques by other people[7],[8]. In the vicinity of the effective anisotropy field H_K, a 6-fold pattern of maxima is seen as $H_{//}$ is rotated through the <110> directions in the plane. Typical data are shown in Fig.8 .

A bump appears at a position which we have marked as $H_{//}=H_{//}^*$ when $H_{//}$ is applied in a <110> direction. This phenomenon can be observed on many samples. The 6-fold symmetry together with the bump were used to align the magnetic field $H_{//}$ in the <110> direction if necessary. The accuracy was believed to be within ±2 degrees.

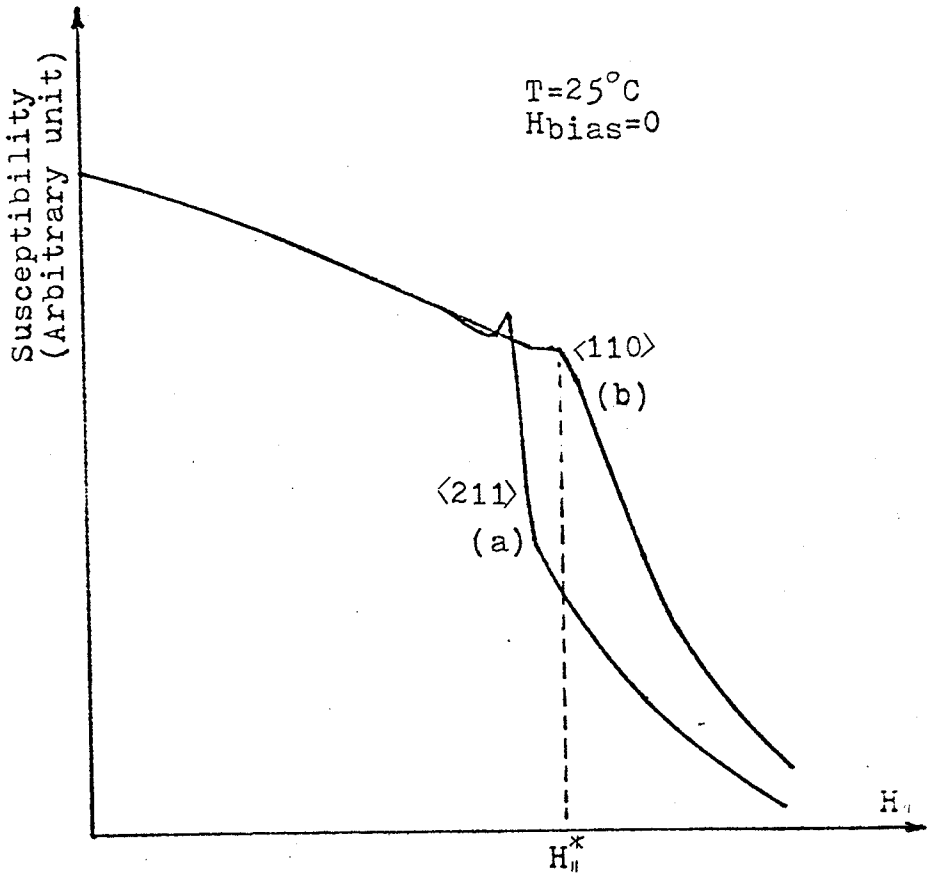

Fig.8 Zero-bias susceptibility data. (a) $H_{//}$ oriented in a <112> direction. (b) $H_{//}$ oriented in a <110> direction in the film plane.

3.2 DOMAIN INSTABILITY WHEN H IS ALONG <110> DIRECTION

With an in-plane magnetic field $H_{//}$ applied along a <110> direction, the total energy per unit volume of the stripe lattice may be written as, with the help of Fig.3,

$$E=\frac{2\sigma}{D}+K_u\cos^2\theta_0-M_sH_{//}\cos\theta_0+K_1\left(\frac{1}{4}\cos^4\theta_0+\frac{1}{3}\sin^4\theta_0\right)+$$

$$+\frac{16\pi M_s^2\sin^2\theta_0}{(1+\sqrt{\mu})\pi^3}\left(\frac{D}{t}\right)\sum_{n=\text{odd}}^{\infty}\left[1-\exp\left(-2n\pi\sqrt{\mu}\frac{t}{D}\right)\right] \qquad (3.1)$$

where

σ---the domain wall energy per unit area

Ku---uniaxial anisotropy constant

K_1---cubic anisotropy constant

$\mu = 1+2\pi Ms/Ku$

for (111) films.

Unlike Druyvesteyn [2], we include the cubic anisotropy energy term in the total energy expression, since we found this term is not negligible compared with other terms when an in-plane field is applied. The last term is the demagnetizing energy due to the free magnetic poles on the film surface. The 'μ-correction' due to the redistribution of the free poles on the film surface caused by internal field is taken into consideration here.

The domain wall energy $\sigma(\theta_0, H_{\parallel}, D/t)$ per unit area of wall, written in general form, is

$$\sigma(\theta_0, H_{\parallel}, D/t) = 2\sqrt{A} \int_{-\theta_0}^{\theta_0} [g(\theta, D/t) - g(\theta_0, D/t) - MsH_{\parallel}\cos\theta + MsH_{\parallel}\cos\theta_0]^{1/2} d\theta \qquad (3.2)$$

where $g(\theta, D/t)$ is the energy term other than the energy of magnetization in a field $H_{\parallel}$ [see Appendix A].

The physical meaning of expression (3.2) is that the domain wall energy is the energy difference between two states with and without the existence of the wall. In principle, we

shall consider all energy terms. In practice,an infinitely thin wall is usually considered, and only the uniaxial anisotropy energy is taken into consideration. This approximation is justified in many cases.In fact, however,the wall has finite width, the magnetization inside the wall rotates from $-\theta_0$ to $+\theta_0$ if we consider the wall as a simple Bloch wall.There is certainly some contribution to the wall energy from demagnetizing energy which has angular dependence as shown in Eq.(3.1). Especially,the magnetization in the centre of the wall contributes nothing to the free magnetic poles on the film surface,nor does it to the demagnetizing energy. It is doubtful that this contribution is small in all cases.After several tries,we found that this contribution is not small when an in-plane field is close to the point where the domains become unstable. As an approximation,we include the uniaxial anisotropy,cubic anisotropy and the demagnetizing energy terms in the function $g(\theta,D/t)$,i.e.,

$$g(\theta,D/t)=K_u\cos^2\theta+K_1\left(\frac{1}{4}\cos^4\theta+\frac{1}{3}\sin^4\theta\right)+$$

$$+\frac{16\pi M_s^2\sin^2\theta}{(1+\sqrt{\mu})\pi^3}\left(\frac{D}{t}\right)\sum_{n=\text{odd}}^{\infty}\frac{1}{n^3}\left(1-\exp\left(-2n\pi\sqrt{\mu}\frac{t}{D}\right)\right) \qquad (3.3)$$

The magnetic moments inside the wall are assumed to be parallel to the X-Y plane. This assumption is not valid for some bubble films, as was reported by A. Hubert et al.[9]. They had observed a roughly perpendicular orientation for

the stripes near the point of instability. However, for simplicity, this possible effect is not taken into consideration here. It may be concluded from our experimental results that it is good enough to use this approximation for the present purpose.

The equilibrium values of θ_0 and the 'lattice constant' D/t can be obtained as a function of $H_{//}$ by equating the first derivatives of E to zero:

$$\frac{\partial E}{\partial \theta_0} = 0 \tag{3.4}$$

$$\frac{\partial E}{\partial (D/t)} = 0 \tag{3.5}$$

Since we are interested in the point of $H_{//}$ where the stripe domains become unstable, we need the third equation, which is,

$$\frac{\partial^2 E}{\partial \theta_0^2}\,\frac{\partial^2 E}{\partial (D/t)^2} - \left(\frac{\partial^2 E}{\partial \theta_0\,\partial (D/t)}\right)^2 = 0 \tag{3.6}$$

to define the unstable condition. In appendix B are given all derivatives of E with respect to θ_0 and D/t. It seems impossible to get an analytical expression for the wall energy term σ by integrating it.However, from the fact that when the stripe domains become unstable, the angle the magnetic dipoles make with the field $H_{//}$ must be small, we can circumvent this difficulty in two ways. One way is to replace $\sin\theta$ by θ, another way is to replace integration by

summation. The latter one is used here because it seems to be more general.

The definition

$$\ell = 4(AKu)^{1/2}/4\pi Ms^2 \qquad (3.7)$$

is the characteristic length defined in the conventional sense. The value of $H_{//}$ used in calculation is nothing but $H_{//}^*$, which can be measured experimentally, corresponding to the point where the stripe domains become unstable since Eq.(3.6) is used. Both $(2Ku/Ms-4\pi Ms)$ and K_1/Ms are obtained from ferromagnetic resonance by using the best fitting technique which will be discussed in Chapter IV. All three equations are solved simultaneously by numerical calculation while both $H_{//}^*/(2Ku/Ms-4\pi Ms)$ and $(K_1/Ms)/H_{//}^*$ are taken as parameters.

A crucial point is the experimental definition of the critical field $H_{//}^*$. As has been seen from Fig.8, a bump appears on the susceptibility curves for many samples if the in-plane field is applied along <110> directions. When the field exceeds the point where the bump appears, the susceptibility behaves hyperbolically with the field. This is the typical behaviour of the rotation of magnetization and is evidence that the domains have disappeared in this region. When the field is below this special point,the magnetization process is mainly by domain wall motion. The behaviour of susceptibility when the field is just below this special point is rather complicated and needs further investigation.

In the present work, the point corresponding to the peak of this bump is assumed as H_{π}^{*} , since, obviously, when the field is larger than this value, the domain structure is removed. The validity of this assumption will be verified by our results. For the samples with no bump on their susceptibility curves, however, the critical field H_{π}^{*} is defined as the point where the susceptibility has the maximum variation; of course, inevitably, the H_{π}^{*} found in this way has a little artificial component.

With the measured values of $H_{\pi}^{*}/(2Ku/Ms-4\pi Ms)$ and $(K_1/Ms)/H_{\pi}^{*}$, the relations between $H_{\pi}^{*}/4\pi Ms$, θ_0, D/t and ℓ/t can be obtained from the numerical calculation. Among these values, only $H_{\pi}^{*}/4\pi Ms$ and ℓ/t are useful for our purpose. We plot $4\pi Ms$ as a function of ℓ/t for a known H_{π}^{*}. A typical curve is shown in Fig.9 .

It is quite interesting to compare Fig.5 with Fig.9. Apparently the curve goes much higher after the modification of the total energy term is made. This gives strong evidence that the cubic anisotropy cannot be neglected. The reason is that other energy terms are getting smaller as θ_0 decreases. It makes the cubic anisotropy energy comparable in magnitude with other terms.

The present calculation is placed on the assumption of Bloch wall structure. But in reality,the wall has twisted wall structure due to the stray surface field. There are

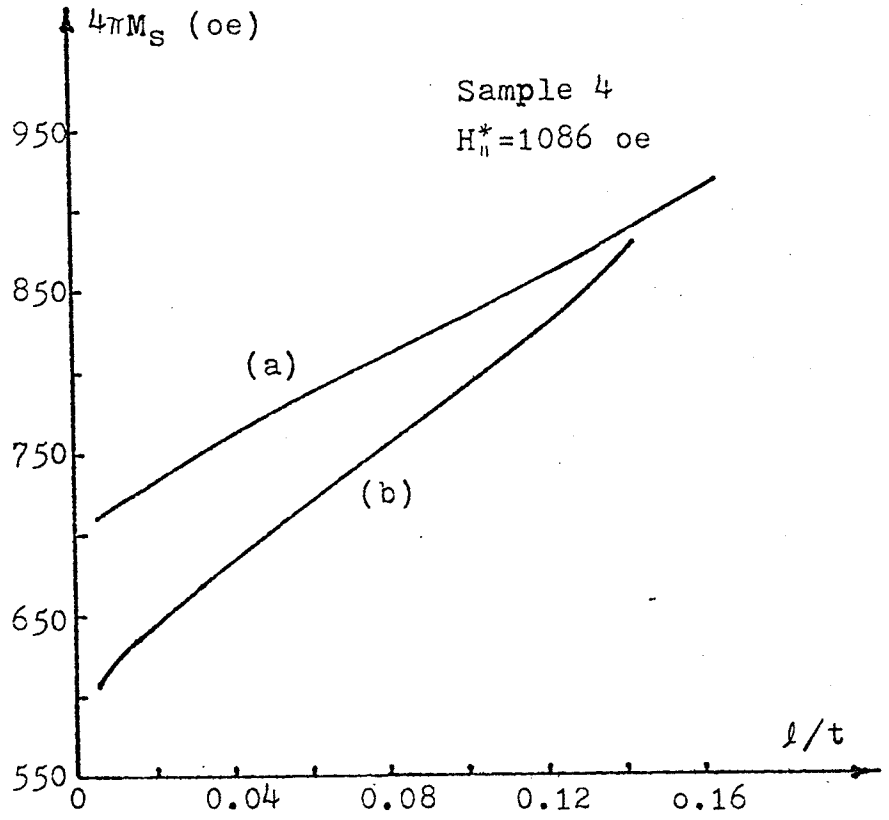

Fig.9 (a) 4πMs versus ℓ/t when $H_{\pi}^{*}/(2Ku/Ms-4\pi Ms)$ =2.44, $(K_1/Ms)/H_{\pi}^{*}$=-0.0442, for the same sample as in Fig.5. The cubic anisotropy is taken into consideration in the total energy term, and both cubic anisotropy and the demagnetizing energy terms are included in domain wall energy, as is shown in Eqs.(3.1)-(3.3).

(b) the curve in Fig.5 where no cubic anisotropy is considered and demagnetizing energy term is neglected in domain wall energy.

many papers [10] dealing with the twist domain wall structures. All the calculations are rather complicated. It is not desired here to go too far in this area. All we have done, as is shown in Eqs. (3.2) and (3.3), has been verified to be sufficient to eliminate the systematic shifts.

3.3 STRIPE DOMAIN COLLAPSE AND INITIAL SUSCEPTIBILITY

The well known theory of Kooy and Enz [1] allows a numerical calculation of the stripe domain collapse field and the initial susceptibility [5]. In this theory, the domain wall energy is assumed to be a constant. If only the uniaxial anisotropy is considered, the wall energy can be expressed as

$$\sigma=4\sqrt{AKu} \tag{3.8}$$

The problem here is to find how much error will be made if, instead of taking Eqs. (3.2) and (3.3) in the limit when $H_{\parallel}=0$, we simply take the expression (3.8) to express the domain wall energy in the case when the magnetic field $H=H_{\perp}$ is applied perpendicular to the plane, i.e., along <111> direction of the films. This definition must be consistent with that in the previous section. In order to have some feel for this, we will start from Eqs. (3.2) and (3.3) to make an estimate.

By setting θ_0 to $\pi/2$ and $H_{\parallel}$ to zero , Eq. (3.2) can be rewritten as

$$\sigma=4\sqrt{AKu}\int_0^{\pi/2}\left[\cos^2\theta+\frac{K_1}{4Ku}\cos^4\theta+\frac{K_1}{3Ku}(\sin^4\theta-1)-\cos^2\theta E_d\right]^{1/2}d\theta \tag{3.9}$$

where

$$E_d=\frac{16\pi Ms^2}{Ku\pi^3(1+\sqrt{\mu})}\frac{D}{t}\sum_{n=odd}^{\infty}\frac{1}{n^3}(1-\exp(-2n\pi\sqrt{\mu}\frac{t}{D})) \qquad (3.10)$$

Defining $x=\cos\theta$, we can rewrite Eq. (3.9) as

$$\sigma=2\sqrt{AKu}\int_0^1[\frac{1-E_d-\frac{K_1}{12Ku}}{1-x^2}-\frac{7K_1}{12Ku}]^{1/2}\,d(x^2) \qquad (3.11)$$

Since

$$|K_1| << Ku,$$

$$|E_D| \sim |K_1/Ku|/12,$$

$$\frac{7\,|K_1|}{12\,Ku} << \frac{1-E_d-\frac{K_1}{12Ku}}{1-x^2}, \qquad 0<x<1$$

for practical films, we can reasonably neglect $7K_1/12Ku$ in the integrand, so we have

$$\sigma\cong 4\sqrt{AKu}[1-E_d-\frac{K_1}{12Ku}]^{1/2}$$

$$\cong 4\sqrt{AKu}[1-\frac{1}{2}(E_d+\frac{1}{12}\frac{K_1}{Ku})]$$

$$=4\sqrt{AKu}\{1-[\frac{1}{24}\frac{K_1}{Ku}+\frac{8\pi Ms^2}{(1+\sqrt{\mu})\pi^3 Ku}\frac{D}{t}\sum_{n=odd}^{\infty}\frac{1}{n^3}(1-\exp(-2n\pi\sqrt{\mu}\frac{t}{D}))]\} \qquad (3.12)$$

It was found that the second term in curly brackets was only a few percent of the first term in magnitude for the samples under test. So it seemed to be unnecessary to include this term in the wall energy. In other words, it is a good approximation to use Eq. (3.8) as the expression of the wall energy in the case when the magnetic field H is applied normal to the films. In this statement, the assumption has been made that the wall energy is independent of the bias field, as was done by Kooy and Enz implicitly.

For this reason, the curve in Fig.2 was used without modification and the relation between $4\pi\chi_0$ and ℓ/t from Maartense et al. were used directly, and is shown in Fig.10 .

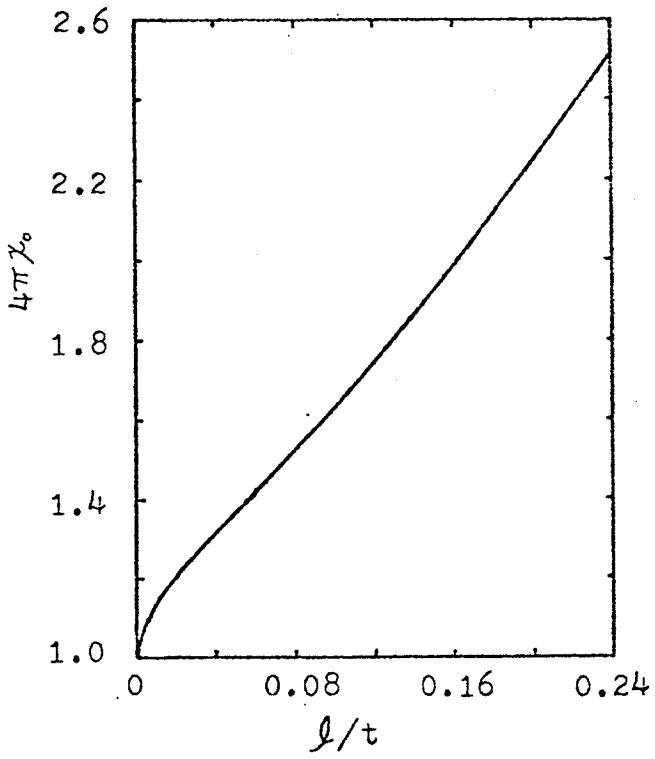

Fig.10 Initial susceptibility as a function of the characteristic-length-to-film-thickness ratio (after Maartense et al.,Ref.5).

Experimentally, the stripe-in field was measured instead of stripe-collapse field. The reason for this is that during stripe collapse, there is large-scale lateral wall motion with considerable coercivity and this, with the possible presence of hard domains, tends to delay and round off the final domain collapse. In contrast, the stripe-in consists initially of rapid stripe-head motion, which usually gives a much sharper change in susceptibility. It is quite safe to consider both fields as the same value in the present context. A typical curve is shown in Fig.11 .

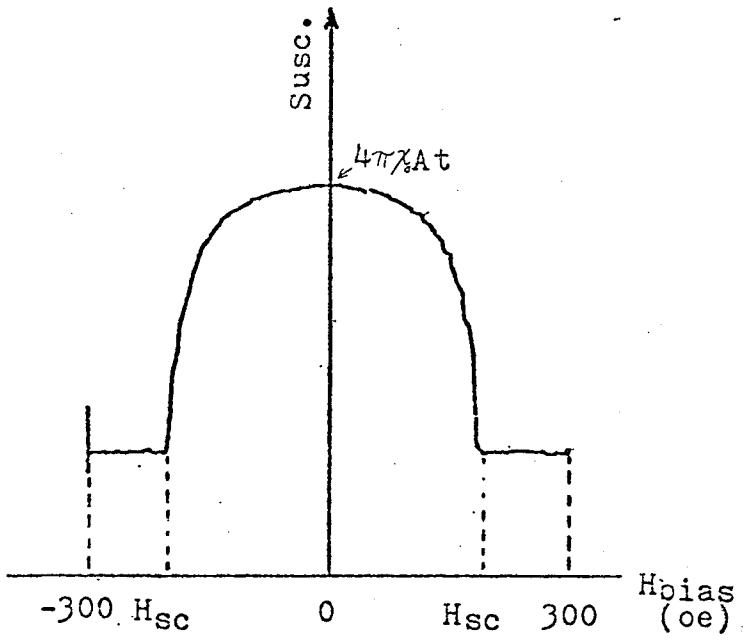

Fig.11 Susceptibility tracing for stripe-in field and initial susceptibility,where A is the area of the film and t is the thickness of the film. For the bubble garnets with films on both sides of the substrates, t must be replaced by 2t.

Because of the finite amplitude of the sensing field, the measured Hsi will be greater than the actual value and $4\pi\chi_0 At$ will be smaller due to the coercivity. So several measurements were made in the condition that the sensing current I_{ac} was changed each time, and then suitable values of the stripe-in field and the initial suscptibility were obtained by linear extrapolation, as was pointed out by Maartense [7].

Fig.12 and Fig.13 give examples of the linear extrapolation.

The theory of Kooy and Enz will be summarized in Appendix C.

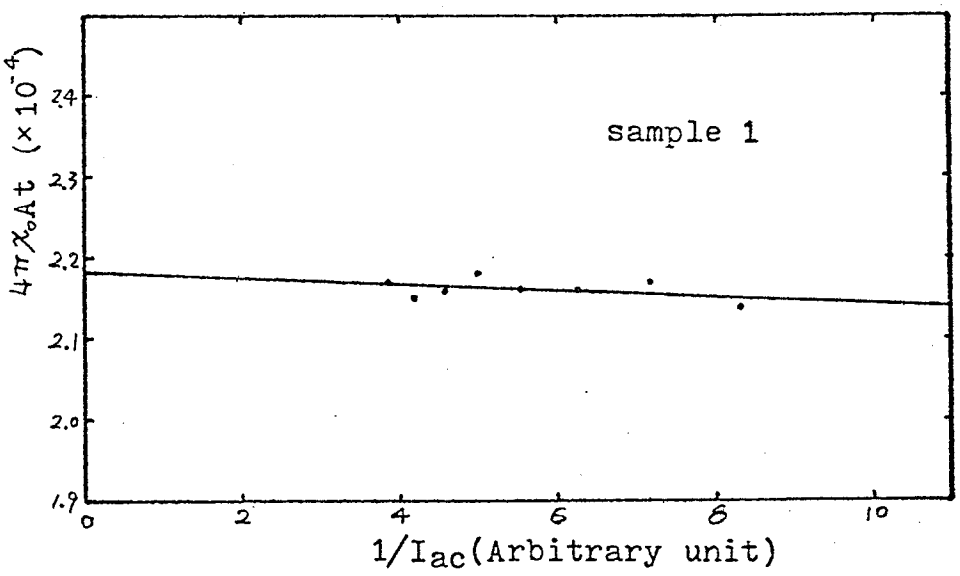

Fig.12 Example of linear extrapolation of $4\pi\chi_0 At(1/I_{ac})$

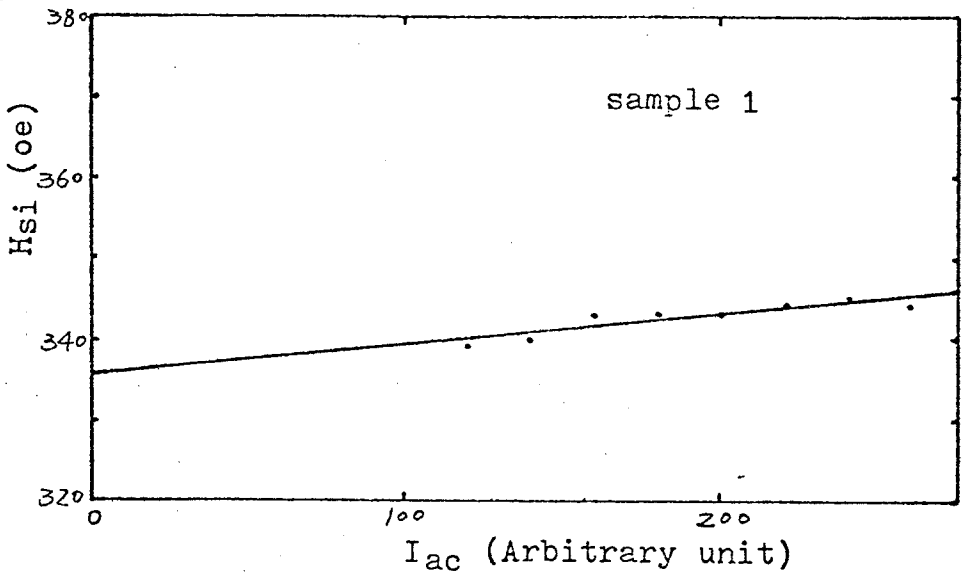

Fig.13 Example of linear extrapolation of Hsi(I_{ac})

Chapter IV

FERROMAGNETIC RESONANCE

Ferromagnetic resonance was first observed by Griffiths [13] in 1946, when he found that the product of the permeability, μ, and the resistance, ρ, of ferromagnetic metals measured in the microwave region had a maximum as the magnetic field strength varied. However, the basic equations were formulated by Landau and Lifshitz [14] in 1935 in their paper on the theory of the dispersion of the permeability in ferromagnetic metals.

When a steady magnetic field is applied, the atomic moments will tend to precess coherently about their equilibrium orientation. It will be assumed that this steady magnetic field is large enough to remove the domain structure. Then the process can be viewed as the precession of the total magnetic moment. Resonance will occur when the frequency of an alternating field applied transversely is equal to the precession frequency.

The equation of motion may be expressed in term of total free energy E [15]. There are several advantages to the en-

ergy formulation of the equations of motion. First, they are more general in form. Second, when the free energy terms are complicated functions of the angular coordinates, they can be introduced routinely into the equations. Third, when the easy directions of the various anisotropies have different orientations, the computations are more straightforward with the energy equations.

Suppose the magnetization $\vec{M}s$ of a ferromagnetic specimen has the static equilibrium direction described by the azimuth ϕ_0 and the polar angle θ_0 , as in Fig.14 . A Lagrangian function, L, can be obtained by considering the magnetic system as a classical top with principal moments of inertia (0,0,c) and Euler angles ϕ, θ, and χ. Here χ is the angle that describes a rotation of the top about its symmetry axis. The angular velocity of the top about this symmetry axis is then $\dot{\chi}$ plus the component of ω_ψ, namely $\dot{\phi}\cos\theta$. The kinetic energy T of the top is therefore given by

$$T=\frac{1}{2}c(\dot{\chi}+\dot{\phi}\cos\theta)^2 \qquad (4.1)$$

and the Lagrangian function by $L=T-E(\theta,\phi)$, where E is the potential energy.

The Lagrange equations of motion have the general form

$$\frac{d}{dt}\left(\frac{\partial L}{\partial \dot{q}}\right)-\frac{\partial L}{\partial q}=0 \qquad (4.2)$$

where q_α is a coordinate. Application of this equation to the present problem yields

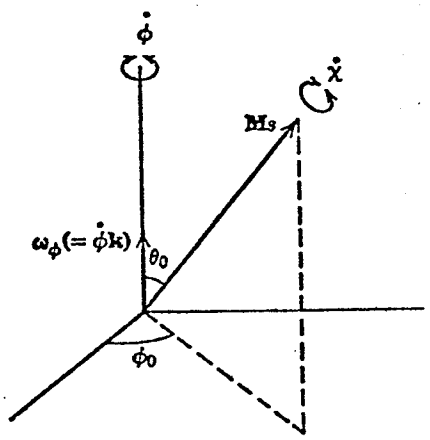

Fig.14 Spherical coordinates for magnetization (after Morrish,Ref.15)

$$\frac{d}{dt}[c(\dot{\chi}+\dot{\phi}\cos\theta)\cos\theta]+\frac{\partial E}{\partial \phi}=0$$

$$c(\dot{\chi}+\dot{\phi}\cos\theta)\dot{\phi}\sin\theta+\frac{\partial E}{\partial \theta}=0$$

$$\frac{d}{dt}[c(\dot{\chi}+\dot{\phi}\cos\theta)]=0$$

From the last of these equations it follows that

$$c(\dot{\chi}+\dot{\phi}\cos\theta)=\text{const.}$$

This constant is no more than Ms/γ in the present case in this approximation, where Ms is the saturation magnetization and $\gamma=ge/2mc$. The equations then become

$$\frac{Ms}{\gamma}\dot{\theta}\sin\theta=\frac{\partial E}{\partial \phi} \qquad (4.3)$$

$$-\frac{Ms}{\gamma}\dot{\phi}\sin\theta=\frac{\partial E}{\partial \theta} \qquad (4.4)$$

Now, suppose that both ϕ and θ deviate from the equilibrium orientation (ϕ_0, θ_0) by small angles $\Delta\theta$ and $\Delta\phi$,

$$\Delta\theta = \varepsilon_\theta e^{i\omega t} \tag{4.5}$$

$$\Delta\phi = \varepsilon_\phi e^{i\omega t} \tag{4.6}$$

where ε_θ and ε_ϕ are small compared with θ_0 and ϕ_0 respectively, hence

$$\sin(\theta_0+\Delta\theta) \cong \sin\theta_0 + \cos\theta_0 \Delta\theta$$

$$\dot{\phi} = i\omega\Delta\phi \tag{4.7}$$

$$\dot{\theta} = i\omega\Delta\theta$$

The energy $E(\theta,\phi)$ may be expanded about the equilibrium position, for which

$$\frac{\partial E}{\partial \phi} = \frac{\partial E}{\partial \theta} = 0$$

$$E(\theta,\phi) \cong E_0 + \frac{1}{2}\left[\left(\frac{\partial^2 E}{\partial \phi^2}\right)_0 (\Delta\phi)^2 + \left(\frac{\partial^2 E}{\partial \theta^2}\right)_0 (\Delta\theta)^2 + 2\left(\frac{\partial^2 E}{\partial\theta\partial\phi}\right)_0 \Delta\phi\Delta\theta\right] \tag{4.8}$$

Substitution of these expressions into equations (4.3) and (4.4) gives to the first order

$$\frac{i\omega M_s}{\gamma}\sin\theta_0\Delta\theta = \left(\frac{\partial^2 E}{\partial\phi^2}\right)_0 \Delta\phi + \left(\frac{\partial^2 E}{\partial\phi\partial\theta}\right)_0 \Delta\theta \quad ,$$

$$-\frac{i\omega M_s}{\gamma}\sin\theta_0\Delta\phi = \left(\frac{\partial^2 E}{\partial\phi\partial\theta}\right)_0 \Delta\phi + \left(\frac{\partial^2 E}{\partial\theta^2}\right)_0 \Delta\theta \quad . \tag{4.9}$$

The resonance frequency can be obtained from this set of homogeneous equations for $\Delta\phi$ and $\Delta\theta$ by setting the determinant of the coefficients to zero. It yields

$$\frac{\omega}{|\gamma|} = \frac{1}{M_s \sin\theta_0}\left[\left(\frac{\partial^2 E}{\partial \phi^2}\right)_0 \left(\frac{\partial^2 E}{\partial \theta^2}\right)_0 - \left(\frac{\partial^2 E}{\partial \phi \partial \theta}\right)_0^2\right]^{1/2} \tag{4.10}$$

When a DC magnetic field is applied in the (110) plane for (111) films, as shown in Fig.15, the total free energy of the system, E, is the sum of Zeeman energy, demagnetizing energy, uniaxial magnetic anisotropy energy and cubic magnetocrystalline anisotropy energy, and is given by

$$E_{total} = -HM_s(\sin\theta\cos\phi\sin\beta + \cos\theta\cos\beta) + 2\pi M_s^2\cos^2\theta + K_u\sin^2\theta +$$
$$+K_1\left(\frac{1}{4}\sin^4\theta + \frac{1}{3}\cos^4\theta + \frac{\sqrt{2}}{3}\sin^3\theta\cos\theta\cos 3\phi\right) \tag{4.11}$$

The contribution from K_2 is neglected in the present calculations (see appendix D).

The equilibrium conditions are found by setting both $\frac{\partial E}{\partial \theta}$ and $\frac{\partial E}{\partial \phi}$ to zero. Equation $\frac{\partial E}{\partial \phi}=0$ always holds when $\phi=0$. This means that $\vec{M}s$ always lies in the (110) plane in which H is applied, since in resonance, H is much larger than the cubic anisotropy field. $\frac{\partial E}{\partial \theta}$ is given by

$$\frac{\partial E}{\partial \theta} = -HM_s\sin(\beta-\theta) + (K_u - 2\pi M_s^2)\sin 2\theta + K_1\left[-\frac{7}{24}\sin 4\theta - \frac{1}{12}\sin 2\theta +\right.$$
$$\left. + \frac{\sqrt{2}}{3}(3\sin^2\theta - 4\sin^4\theta)\right] \tag{4.12}$$

The second derivatives $\frac{\partial^2 E}{\partial \theta^2}$, $\frac{\partial^2 E}{\partial \phi^2}$ and $\frac{\partial^2 E}{\partial \theta \partial \phi}$ are substituted into Eq. (4.10). Then the resonance condition is given by

$$\frac{\omega}{\gamma} = \frac{1}{M_s \sin\theta}[\{HM_s\cos(\beta-\theta)+2(K_u-2\pi M_s^2)\cos 2\theta+K_1(-\frac{7}{6}\cos 4\theta-\frac{1}{6}\cos 2\theta+$$

$$+\frac{\sqrt{2}}{3}\sin 2\theta(3-8\sin^2\theta))\}\cdot(HM_s\sin\theta\sin\beta-3\sqrt{2}K_1\sin^3\theta\cos\theta)]^{\frac{1}{2}} \qquad (4.13)$$

under the restriction of Eq. (4.12) being equal to zero.

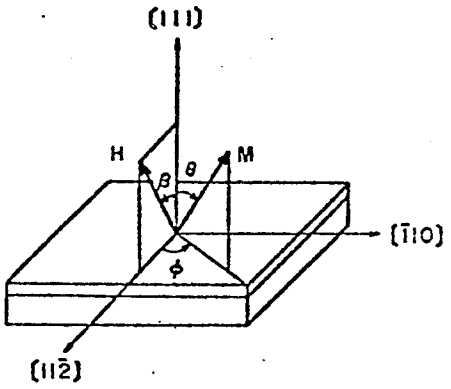

Fig.15 Coordinate system for (111) film. H is applied in (110) (after Hiroshi,Ref.17).

Specifically,perpendicular and parallel resonance conditions have been determined and given by [16]

1. H // [111] film normal

$$\frac{\omega}{|\gamma|} = H_\perp + (\frac{2K_u}{M_s} - 4\pi M_s) - \frac{K_1}{M_s} \qquad (4.14)$$

2. H // [112] in-plane

$$\left(\frac{\omega}{|\gamma|}\right)^2 = H_{\parallel}\left\{H_{\parallel} - \left(\frac{2Ku}{Ms} - 4\pi Ms\right) - \frac{K_1}{Ms}\right\} \qquad (4.15)$$

Then, both $(2Ku/Ms - 4\pi Ms)$ and K_1/Ms are obtained by a best-fitting method [17]. The experimental data are analyzed by making use of a computer program based on the following procedure.

1. A set of initial values of K_1/Ms, $H_{\perp}$ and $H_{\parallel}$ is used to calculate $(2Ku/Ms - 4\pi Ms)$ and $\omega/|\gamma|$ values through Eqs.(4.14) and (4.15).
2. Hres values are calculated for each β between 10° and 170° by solving Eq. (4.13) under the condition of Eq. (4.12) being zero, without using any experimental Hres values for β=10°-170°.
3. The coincidence between calculated and experimental data is judged by introducing a total error sum for each field orientation

$$\Sigma(\text{error})^2 = \sum_{\beta=0^0}^{170^0} (H_{res.}^{cal.} - H_{res.}^{exp.})^2$$

By changing K_1/Ms, $\Sigma(\text{error})^2$ is calculated and plotted as a function of K_1/Ms and β. The values of $(2Ku/Ms - 4\pi Ms)$ and K_1/Ms corresponding to the minimum $\Sigma(\text{error})^2$ are to be considered as the best fitting ones.

The method of magnetic alignment was used to find <110> directions for each sample before the resonance experiment was done,as discussed in section (3.1). Then the resonance field Hres was recorded at each angle β from 0° to 170°. Fig.16 shows typical results of the resonance.

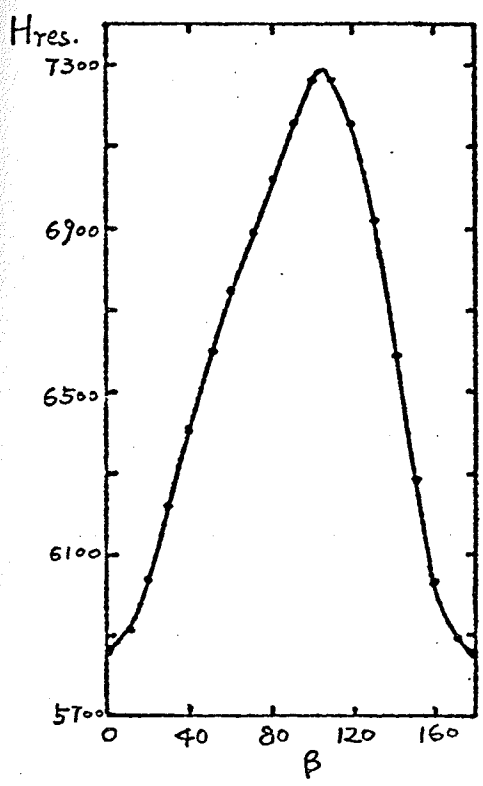

(a) Resonance field orientation dependence.

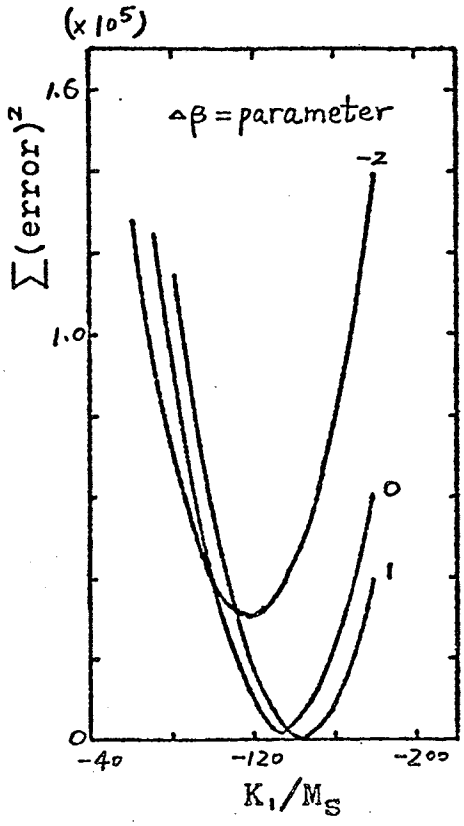

(b) Error sum K_1/Ms dependence.

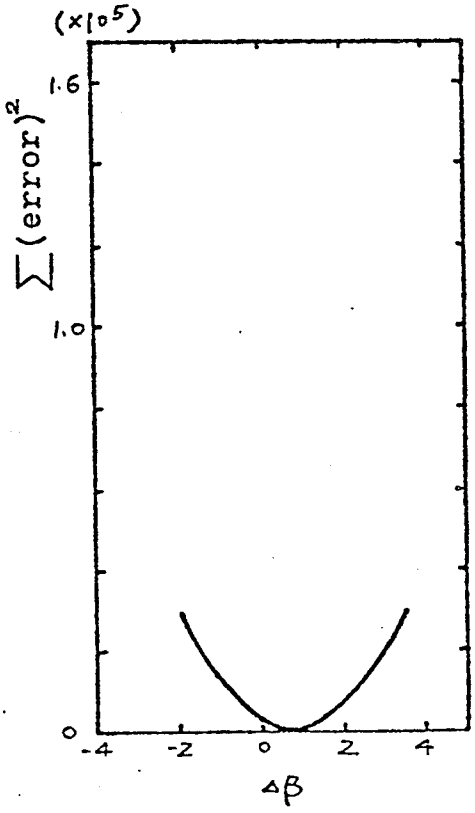

(c) Error sum $\Delta\beta$ dependence.

Fig.16 Illustration of the best fitting method.

The angle β is shifted backwards or forwards by the amount of $\Delta\beta$ to eliminate sample misalignment effect.

The best fitting values are: $K_1/Ms=-141$,

$2Ku/Ms-4\pi Ms=788$,

for sample 3.

Chapter V

OPTICAL THICKNESS OF THE FILM

The samples used here have films on both sides of the substrates. Two such films on one substrate are believed, at least in a good approximation, to have the same thickness and composition. A modified model similar to Manifacier's [18] is set up to analyze the transmission spectrum. We will follow Rouard's treatment [19] and consider only the normal incidence case.

Now, consider the structure in Fig.17 where the number 3 and 3' represent air environment, 2 and 2', films, and 1, substrate.

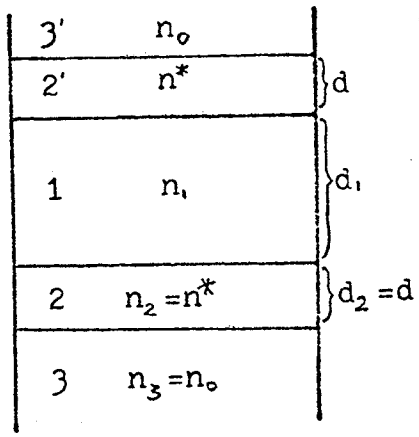

Figure 17 Structure of the films, $n^*=n-ik$.

The assumption made here is

$$d_1 >> d \tag{5.1}$$

which is valid for all practical films. To calculate the total transmission coefficient, we will start from the interfaces 2-3 and 1-2 to obtain the effective reflection and transmission coefficients for layer 2, i.e., to replace layer 2 by the effective coefficients. Then, to replace the layer 1, and so on until we get the total transmission coefficient. The notations used are

r---reflection

t---transmission

For simplicity, the substrates are assumed to be non-absorbing. There is no doubt about the validity of this assumption.

The Fresnel coefficients shown in Fig.18 are

$$r_2=\frac{n_1-n^*}{n_1+n^*}$$

$$r_3=\frac{n^*-n_0}{n^*+n_0} \tag{5.2}$$

$$t_2=\frac{2n_1}{n_1+n^*}$$

$$t_3=\frac{2n^*}{n^*+n_0}$$

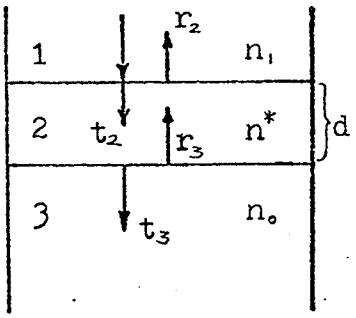

Fig.18 Fresnel coefficients for layers 1,2 and 3

The change in phase of the beam on traversing the film 2 is

$$\delta_2 = \frac{2\pi dn^*}{\lambda} \qquad (5.3)$$

where λ is the wavelength of the incident light in vacuum. The reflected amplitude from the interface 1-2 is given by

$$R_{12} = \frac{r_2 + r_3 e^{-2i\delta_2}}{1 + r_2 r_3 e^{-2i\delta_2}} \qquad (5.4)$$

The transmitted amplitude from the interface 2-3 is given by

$$T_{23} = \frac{t_2 t_3 e^{-2i\delta_2}}{1 + r_2 r_3 e^{-2i\delta_2}} \qquad (5.5)$$

Now, the layer 2 is equivalent to an interface with the effective Fresnel coefficients R_{12} and T_{23}, as is shown in Fig.19 .

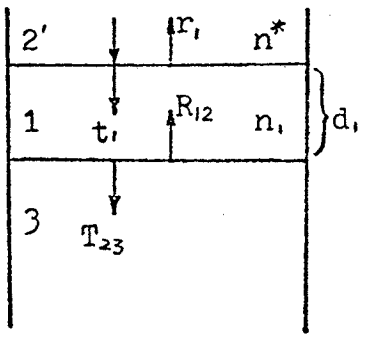

Fig.19 Equivalent interface with effective Fresnel coefficients

The reflected amplitude from interface 1-2' is

$$R_{12}' = \frac{r_1 + R_{12} e^{-2i\delta_1}}{1 + r_1 R_{12} e^{-2i\delta_1}} \qquad (5.6)$$

with

$$\delta_1 = \frac{2\pi n_1 d_1}{\lambda}$$

$$r_1 = \frac{n^* - n_1}{n^* + n_1} \qquad (5.7)$$

The transmitted amplitude from interface 1-3 is given by

$$T_{13} = \frac{t_1 T_{23} e^{-i\delta_1}}{1 + r_1 R_{12} e^{-2i\delta_1}} \qquad (5.8)$$

where

$$t_1 = \frac{2n^*}{n^* + n_1}$$

By making use of (5.4) and (5.5), we can eliminate R_{12} and T_{23} in (5.6) and (5.8) respectively. It gives

$$R_{1\acute{2}} = \frac{r_1 + r_2 e^{-2i\delta_1} + r_3 e^{-2i(\delta_1+\delta_2)} + r_1 r_2 r_3 e^{-2i\delta_2}}{1 + r_1 r_2 e^{2i\delta_1} + r_2 r_3 e^{-2i\delta_2} + r_1 r_3 e^{-2i(\delta_1+\delta_2)}} \qquad (5.9)$$

$$T_{13} = \frac{t_1 t_2 t_3 e^{-i(\delta_1+\delta_2)}}{1 + r_2 r_3 e^{-2i\delta_2} + r_1 r_2 e^{-2i\delta_1} + r_1 r_3 e^{-2i(\delta_1+\delta_2)}} \qquad (5.10)$$

Now, only one layer 2' is left with a bottom interface which has the effective Fresnel coefficients R_{12}' and T_{13}, as shown in Fig.20.

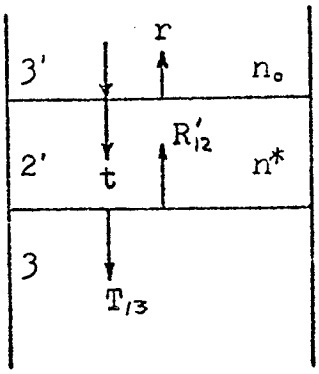

Fig.20 Equivalent interface with effective Fresnel coefficients

The Fresnel coefficients in this case are

$$r=\frac{n_0-n^*}{n_0+n^*}$$

$$t=\frac{2n_0}{n_0+n^*} \qquad (5.11)$$

and the phase change is

$$\delta=\frac{2\pi n^* d}{\lambda} \qquad (5.12)$$

The total reflective amplitude of light of the system is given as

$$R=\frac{r+R_{12}'e^{-2i\delta}}{1+rR_{12}'e^{-2i\delta}} \qquad (5.13)$$

Similarly, the total transmitted amplitude of the light traveling through the system is

$$T_t=\frac{tT_{13}e^{-i\delta}}{1+rR_{12}'e^{-2i\delta}} \qquad (5.14)$$

With the help of Eqs. (5.9) and (5.10), we find

$$\begin{aligned}R=[&r+rr_1r_2e^{-2i\delta_1}+rr_2r_3e^{-2i\delta_2}+rr_1r_3e^{-2i(\delta_1+\delta_2)}+r_1e^{-2i\delta}+\\&+r_2e^{-2i(\delta_1+\delta)}+r_3e^{-2i(\delta_1+\delta_2+\delta)}+r_1r_2r_3e^{-2i(\delta_2+\delta)}]/[1+\\&+r_1r_2e^{-2i\delta_1}+r_2r_3e^{-2i\delta_2}+r_1r_3e^{-2i(\delta_1+\delta_2)}+rr_1e^{-2i\delta}+\\&+rr_2e^{-2i(\delta+\delta_1)}+rr_3e^{-2i(\delta_1+\delta_2+\delta)}+rr_1r_2r_3e^{-2i(\delta_2+\delta)}] \qquad (5.15)\end{aligned}$$

and

$$T_t=[tt_1t_2t_3e^{-i(\delta+\delta_1+\delta_2)}]/[1+r_1r_2e^{-2i\delta_1}+r_2r_3e^{-2i\delta_2}+$$

$$+r_1r_3e^{-2i(\delta_1+\delta_2)}+rr_1e^{-2i\delta}+rr_2e^{-2i(\delta_1+\delta)}+$$

$$+rr_3e^{-2i(\delta+\delta_1+\delta_2)}+rr_1r_2r_3e^{-2i(\delta_2+\delta)}] \qquad (5.16)$$

Noticing that

$$\delta=\delta_2$$

$$r=-r_3$$

$$r_1=-r_2 \quad ,$$

We can rewrite T_t as

$$T_t=[tt_1t_2t_3e^{-i(2\delta+\delta_1)}]/[1-r_1^2e^{-2i\delta_1}+2rr_1e^{-2i\delta}-$$

$$-2rr_1e^{-2i(\delta+\delta_1)}-r^2e^{-2i(2\delta+\delta_1)}+r^2r_1^2e^{-4i\delta}] \qquad (5.17)$$

The transmittance is defined as

$$T=|T_t|^2 \qquad (5.18)$$

and the optical parameter is

$$n^*=n-ik \qquad (5.19)$$

where k is an extinction coefficient.

Because d_1 satisfies the condition $d_1 >> d$, when the frequency of the incident light changes by a small amount Δf, which corresponds to a small change of the wavelength λ, δ_1 will change rapidly while δ remains almost constant. If we average the exponential terms with respect to the wavelength

of the incident light, all terms related to δ_1 will be averaged to zero. In this way, we find the expression for T is

$$T=\frac{|t|^2|t_1|^2|t_2|^2|t_3|^2\alpha^2}{DE} \tag{5.20}$$

with

$$\alpha=\exp(-4\pi kd/\lambda)$$

and

$$\begin{aligned}DE=&1+|r_1|^4+8|r|^2|r_1|^2\alpha^2+|r|^4\alpha^4+|r|^4|r_1|^4\alpha^4+\\&+\alpha[(2r^*r_1^{\dagger}+2|r_1|^2r_1r^*)e^{2i\delta'}+(2rr_1+2|r_1|^2rr_1^{\dagger})e^{-2i\delta'}]+\\&+\alpha^2[(r_1^2r^{*2}+r^{*2}r_1^{\dagger 2})e^{4i\delta'}+(r^2r_1^{\dagger 2}+r^2r_1^2)e^{-4i\delta'}]+\\&+\alpha^3[(2|r|^2|r_1|^2r^*r_1^{\dagger}+2|r|^2r_1r^*)e^{2i\delta'}+(2|r|^2rr_1^{\dagger}+\\&+2|r|^2|r_1|^2rr_1)e^{-2i\delta'}]\end{aligned} \tag{5.21}$$

where

$$\delta'=\frac{2\pi nd}{\lambda}$$

With the conditions, which are satisfied for the samples under test,

$$\begin{aligned}&k^2 \ll (n-n_1)(n_0-n)\ ,\\&k^2 \ll (n+n_1)(n_0+n)\ ,\\&k^2 \ll (n_0+n)^2\ ,\\&k^2 \ll n^2\ ,\\&k^2 \ll (n_0-n)^2\ ,\\&k^2 \ll (n_1+n)^2\ ,\\&k^2 \ll (n-n_1)^2\ ,\end{aligned} \tag{5.22}$$

we obtain the final expression for transmittance T

$$T=(16n_0n^2n_1\alpha)^2/\{[(n+n_0)^2(n_1+n)^2+(n-n_0)^2(n_1-n)^2\alpha^2+$$
$$+2(n+n_0)(n_1+n)(n-n_0)(n_1-n)\alpha\cos(\frac{4\pi nd}{\lambda})]^2+[(n+n_0)^2(n-n_1)^2+$$
$$+\alpha^2(n+n_1)^2(n_0-n)^2+2\alpha(n+n_1)(n+n_0)(n-n_1)(n_0-n)\cos(\frac{4\pi nd}{\lambda})]^2\} \qquad (5.23)$$

By making comparison with the expression of transmittance for single layer films [18], we find that T is not a simple square of the one for single layer films. The second term in the denominator in (5.23), however, is small in magnitude compared with the first term. For the samples under consideration,

$$n > n_0 ,$$

$$n > n_1 ,$$

so

$$n_1 - n < 0 ,$$

$$n - n_0 > 0 .$$

When

$$\frac{4\pi nd}{\lambda}=p2\pi \qquad ,p=0,1,2,\cdots \qquad (5.23')$$

then, $$\cos(\frac{4\pi nd}{\lambda})=1$$

and

$$T_{max}=(16n_0n_1n^2\alpha)^2/\{[(n+n_0)(n_1+n)+\alpha(n-n_0)(n_1-n)]^4+$$

$$+[(n+n_0)(n-n_1)+\alpha(n+n_1)(n_0-n)]^4\} \qquad (5.24)$$

When

$$\frac{4\pi nd}{\lambda}=(2p+1)\pi\ ,\quad p=0,1,2,\cdots \qquad (5.24')$$

then $$\cos(\frac{4\pi nd}{\lambda})=-1\ ,$$

and

$$T_{min}=(16n_0n_1n^2\alpha)^2/\{[(n+n_0)(n_1+n)-\alpha(n-n_0)(n_1-n)]^4+$$

$$+[(n+n_0)(n-n_1)-\alpha(n+n_1)(n_0-n)]^4\} \qquad (5.25)$$

The ratio of T_{max} and T_{min} is

$$\frac{T_{max}}{T_{min}}=\frac{[(n+n_0)(n_1+n)-\alpha(n-n_0)(n_1-n)]^4+[(n+n_0)(n-n_1)-\alpha(n+n_1)(n_0-n)]^4}{[(n+n_0)(n_1+n)+\alpha(n-n_0)(n_1-n)]^4+[(n+n_0)(n-n_1)+\alpha(n+n_1)(n_0-n)]^4} \qquad (5.26)$$

The thickness of each film can be calculated from (5.23')

$$d=\frac{M\lambda_1\lambda_2}{2[n(\lambda_1)\lambda_2-n(\lambda_2)\lambda_1)} \qquad (5.27)$$

where M is the number of oscillations between two extrema.

To analyse the transmission spectrum, we follow the way Manifacier et al. proposed [18]. We consider T_{max} and T_{min} as continuous functions of λ through $n(\lambda)$ and $\alpha(\lambda)$. These, which are the envelopes of the maxima $T_{max}(\lambda)$ and the minima $T_{min}(\lambda)$ in the transmission spectrum are shown in Fig.21 .

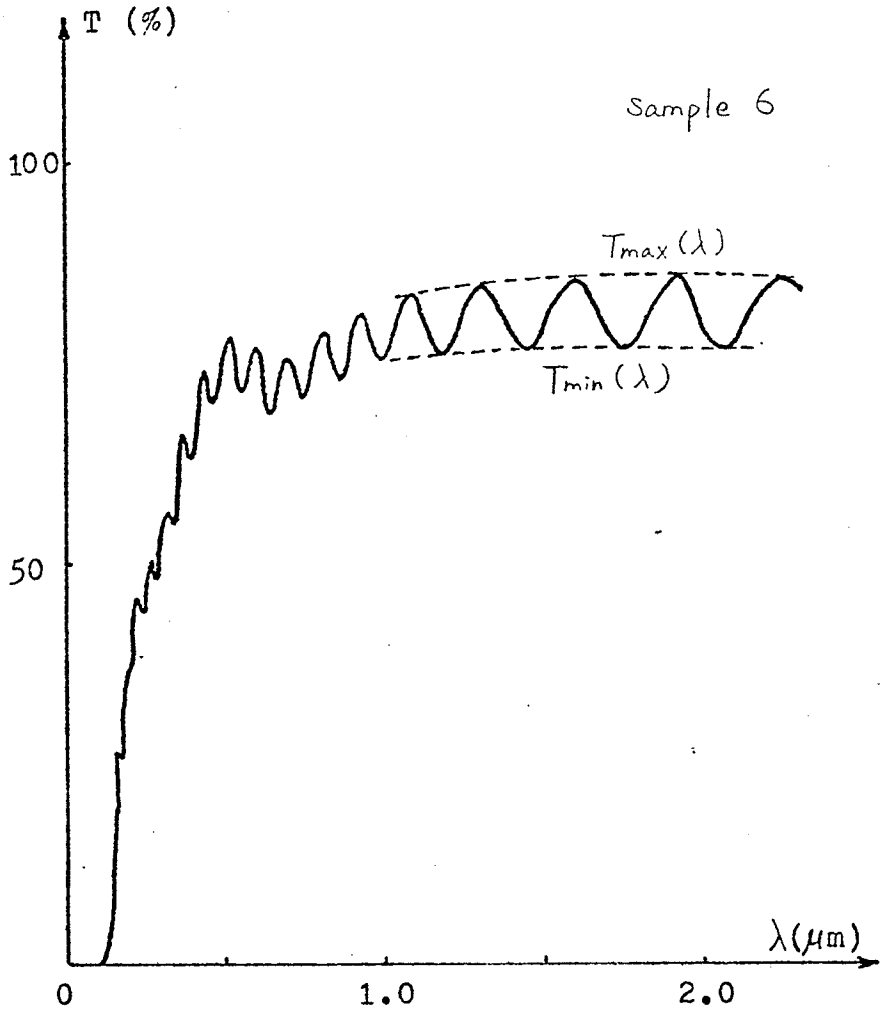

Fig.21 Typical transmission spectrum for a thin bubble film of thickness t=1.9 μm.

The refractive indices n_1 of the substrates were obtained from the dispersion equation [20] for $Gd_3Ga_5O_{12}$ material

$$n_1^2-1=E_d E_0/(E_0^2-E^2) \qquad (5.28)$$

with

$$E_d=25.7 \text{ eV} ,$$

E_0=9.4 eV

and E is the energy of the incident photons in eV. From this equation, n_1=1.935 when λ=2μm; n_1=1.941 when λ=1.2μm.

The values of the α's and n's are obtained by solving, simultaneously, Equs. (5.24) and (5.26) numerically. Then the thickness of the film is calculated from Equ. (5.27). The long wavelength region will be used to minimize the errors because the absorption occurs in the ultraviolet region. The refractive indices n obtained from this model are very close to those obtained from the single layer model [18], the relative difference, $\Delta n/n$, being less than one percent. The relative difference, $\Delta t/t$, in thickness agrees within 2 % .

Chapter VI

THICKNESS OF THE FILM BY WHOLLY MAGNETIC MEASUREMENT

Combining Fig.2 and Fig.9, we will be able to find the intersection of two lines, as is illustrated in Fig.22 .

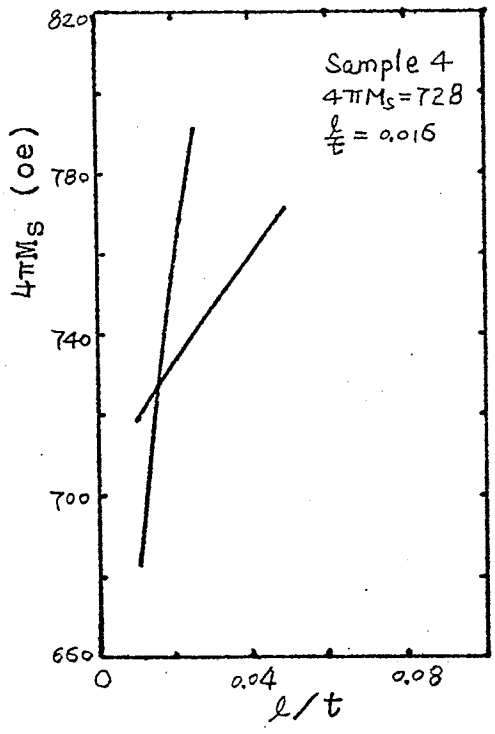

Fig.22 Saturation magnetization and normalized characteristic length obtained magnetically.

With ℓ/t obtained graphically, we can find $4\pi\chi_0$ from Fig.10, and then we are able to calculate the thickness t,

$$t = \frac{(2tA \cdot 4\pi\chi_0)}{2A(4\pi\chi_0)} \quad , \tag{6.1}$$

where $(2tA4\pi\chi_0)$ is the susceptibility of the whole film from the susceptibility measurement and A is the measured area of the film. The factor 2 comes from the fact that there are films on both sides of the substrate.

Now we have obtained the magnetic parameters ℓ/t, Ms, t, $2Ku/Ms-4\pi Ms$, K_1/Ms, and $4\pi\chi_0$, so it is quite easy to calculate other parameters such as Ku, K_1, ℓ, D and Hc, the bubble collapse field .

In total, eight samples were tested and the results are shown in Table 1 and Table 2 . The relative differences defined by

$$\Delta = \frac{|t_{opt.} - t_{mag.}|}{t_{opt.}}$$

are also shown in Table 2.

The stripe collapse field Hsc and the in-plane field $H_{\parallel}^{*}$ where the domains become unstable are listed in Table 3 . The deviation of $H_{\parallel}^{*}$ from $2Ku/Ms$ and $2Ku/Ms+K_1/Ms$ are shown in Table 4 .

The most interesting thing is to see how good the agreement is between the thickness values obtained from two dif-

TABLE 1

Static magnetic parameters obtained wholly magnetically

sample number	t (μm)	4πMs (Oe)	ℓ/t	$4\pi\chi_0$	2Ku/Ms-4πMs(Oe)	K_1/Ms (Oe)
1	2.61	583	0.043	1.33	461	-66
2	12.4	335	0.023	1.22	1275	-108
3	4.92	279	0.082	1.53	788	-141
4	2.57	728	0.016	1.18	446	-48
5	2.73	496	0.128	1.79	1636	-100
6	2.09	514	0.019	1.20	302	-32
7	2.10	489	0.23	2.47	1446	-92
8					1140	-120

ferent experimental methods, since the thickness is the only parameter which is measured independently.In this way, we can verify the validity of the theories of domain stability. From table 2, it is obvious that for most samples, the agreements are good. But for sample 7, the relative error is too large to make the data acceptable. The probable source of this error is believed, however, to be the bad background of the resonance spectrum which makes it difficult to pick up the resonance positions correctly, so that the unreliable values of both 2Ku/Ms-4πMs and K_1/Ms for this sample are responsible for the large discrepancy. For sample 8, it was found that the θ_0 at the point of instability was so small

TABLE 2

Static magnetic parameters(thicknesses obtained optically)

sample number	t (μm)	4πMs (Oe)	ℓ/t	$4\pi\chi_0$	Δ (%)	n (λ=1.6μm)
1	2.52	588	0.047	1.37	3.6	2.07
2	12.1	373	0.039	1.26	2.5	2.04
3	4.75	272	0.09	1.59	3.6	2.06
4	2.62	685	0.014	1.16	1.9	2.09
5	2.89	442	0.098	1.69	5.5	2.11
6	1.89	575	0.035	1.33	11.0	2.08
7	2.84	304	0.115	1.83	26.0	2.06
8	9.07	229	0.058	1.40		2.01

TABLE 3

Hsc and $H_{\parallel}^{*}$ for different samples

sample	1	2	3	4	5	6	7	8
Hsc(Oe)	335	224	129	520	186	354	117	120
$H_{\parallel}^{*}$(Oe)	922	1473	893	1086	1959	750	1725	1198

that the computer had a hard time to search for the correct answers. We may consider these two examples as exceptions. It seems to be reasonable to reject them.

TABLE 4

Deviation of $H_{//}^{*}$ from 2Ku/Ms and 2Ku/Ms+K_1/Ms

sample	1	2	3	4	5	6	7
2Ku/Ms-$H_{//}^{*}$	122	137	174	88	173	66	210
H_K-$H_{//}^{*}$ *	56	29	33	40	73	34	118

* H_K=2Ku/Ms+K_1/Ms , from Table 1.

We can see that the discrepancy in ℓ/t is larger than that in thickness. This is to be expected since $\Delta(\ell/t)$ is a combination of $\Delta\ell$ and Δt in some way, and the $\Delta\ell$ is related to $\Delta(4\pi Ms)$.

It is worthwile to mention that if the demagnetizing energy were not included in the domain wall energy expression, the relative differences would have almost a linear relation with D/t. This strong evidence shows that the demagnetizing energy must be included in the domain wall energy in our case, even in a simple way, although it will result in a tedious calculation inevitably. Fig.23 shows the relation between $(t_{mag.}-t_{opt.})/t_{opt.}$ and D/t in two cases with and without demagnetizing energy in the domain wall energy respetively.

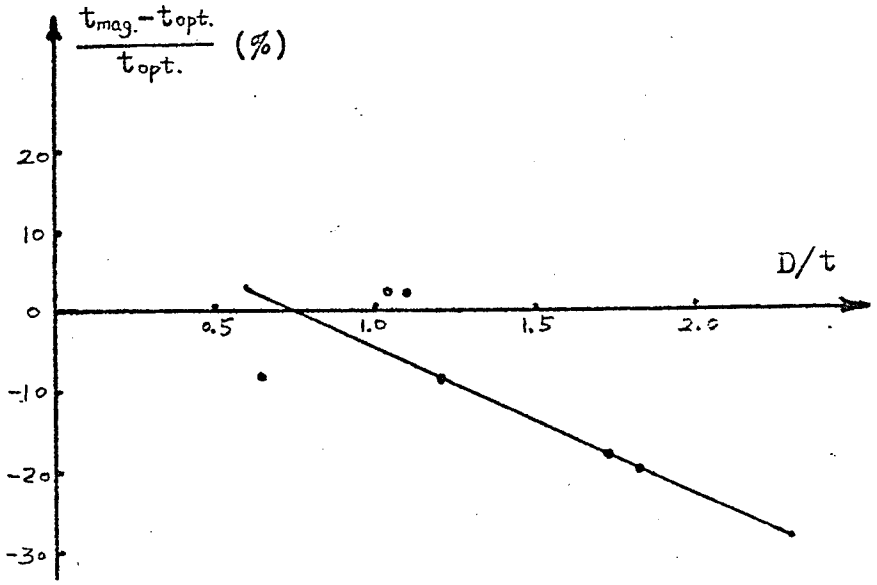

(a)

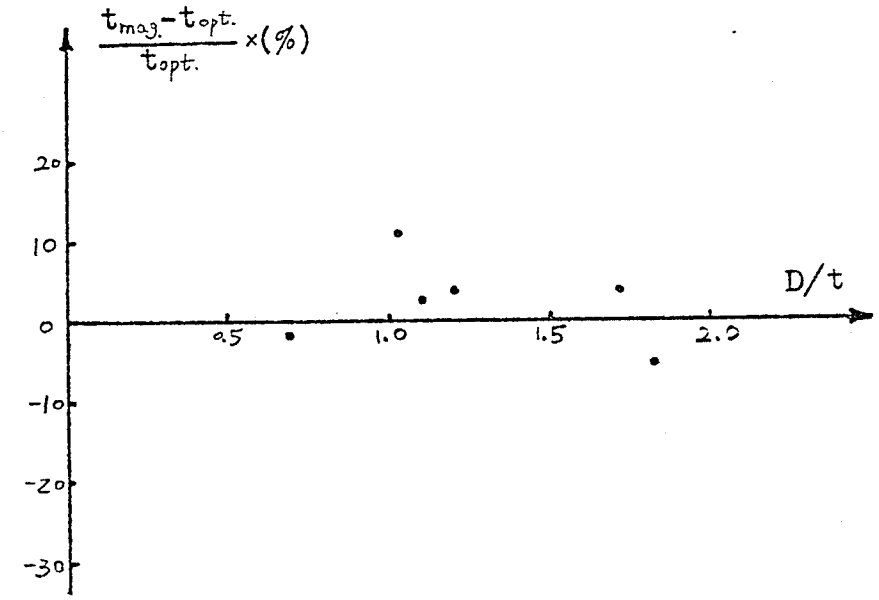

(b)

Fig.23 Relative error in thickness versus D/t. (a) Demagnetizing energy is not included in the wall energy. (b) Demagnetizing energy is included in the wall energy.

Chapter VII

ERROR ANALYSIS

7.1 ERRORS IN MAGNETIC MEASUREMENTS

Besides experimental error sources such as reading errors, temperature fluctuations, etc., the method itself has the disadvantage of propagating the experimental errors with magnification greater than 1 when $H_{//}^{*}/(2Ku/Ms-4\pi Ms)$ is very small. To see this, we plot the relations between $H_{//}^{*}/(2Ku/Ms-4\pi Ms)$ and $H_{//}^{*}/4\pi Ms$ for a typical value of $K_1/MsH_{//}^{*}$, as is shown in Fig.24. To simplify the calculation, the cubic anisotropy and the demagnetizing energy are not included in the domain wall energy when calculating these curves. It is believed that this simplification only causes the curves to shift to the left side with respect to the ones without the simplification. These curves are good enough for error analysis purposes. Approximately, when $H_{//}^{*}/(2Ku/Ms-4\pi Ms)$ is less than 1.1, a small error in $H_{//}^{*}/(2Ku/Ms-4\pi Ms)$ will result in a large error in $H_{//}^{*}/4\pi Ms$ which will be used to calculate $4\pi Ms$. The problem is even more serious when $H_{//}^{*}/(2Ku-4\pi Ms)$ is about 1.0. Fortunately, however, the values of $H_{//}^{*}/(2Ku/Ms-4\pi Ms)$ are not as small as 1.0 for most practical bubble films. For the samples under

test, these values range from 1.13 to 2.45,so this problem is not serious.

It was found, by changing $H_{//}^*$ deliberately, that the accuracy of $H_{//}^*$ indeed has big effects on the vertical position of the lines illustrated in Fig.9. The errors in $H_{//}^*$ may be amplified several times, depending on the value of $H_{//}^*/(2Ku/Ms-4\pi Ms)$. The quantitative analysis is, however, impractical because of the complexity of the equations.

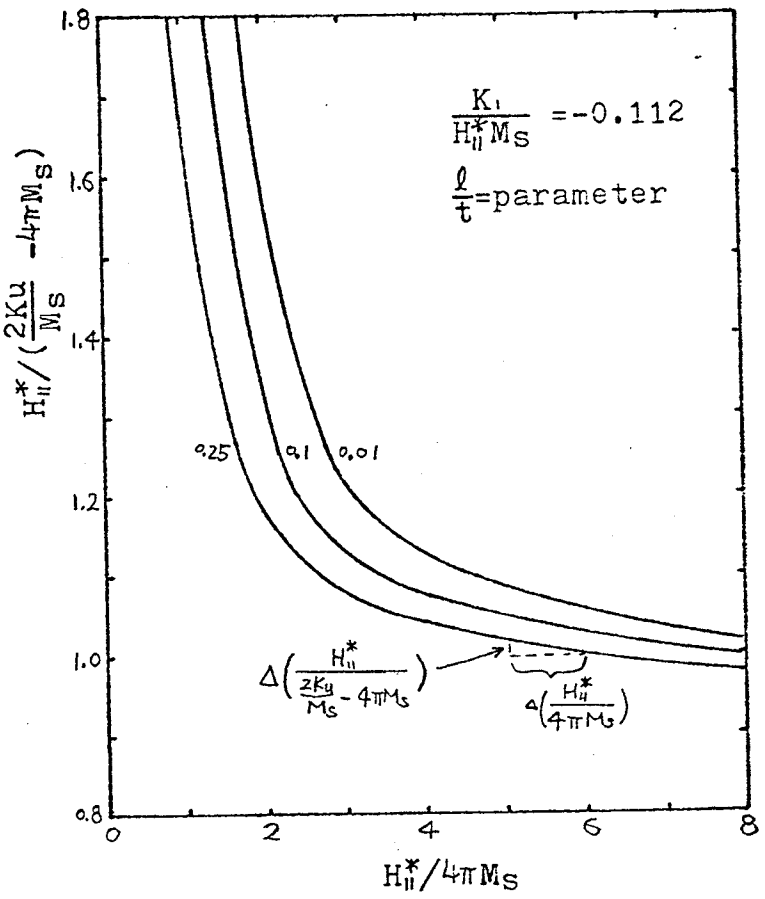

Fig.24 Illustration of the way in which the error propagates

In measuring $H_{\parallel}^{*}$, we took the data for $H_{\parallel}^{*}$ at six positions of the azimuthal angle, each $\pi/3$ apart. The average of $H_{\parallel}^{*}$ was obtained by summing all $H_{\parallel}^{*}$'s and then dividing the summation by six. The uncertainty of $H_{\parallel}^{*}$ was estimated to be less than one percent. The errors in Hsc and $4\pi\chi_0$At were estimated to be one percent or less. The fact that the 'μ' correction was not considered in the calculation of Hsc is one of the error sources, but this effect is believed to be negligible. The error in measuring the area of the films is within 2% .

7.2 ERRORS IN OPTICAL MEASUREMENT

The refractive indices of the films, n, are in the range between 2.00 and 2.10, and that of the substrate, n_1, from 1.93 to 1.94. As a result, the second term in the denominators in Eqs. (5.24) and (5.25) are much smaller than the first term. Therefore, Eqs. (5.24) and (5.25) may be simplified by neglecting the second term in the denominator to yield

$$T_{max} \cong \frac{(16n_0n_1n^2\alpha)^2}{[(n+n_0)(n_1+n)+\alpha(n-n_0)(n_1-n)]^4} \tag{7.1}$$

and

$$T_{min} \cong \frac{(16n_0n_1n^2\alpha)^2}{[(n+n_0)(n_1+n)-\alpha(n-n_0)(n_1-n)]^4} \tag{7.2}$$

for the convenience of error analysis.

The combination of Eqs. (7.1) and (7.2) will give the expression for α,

$$\alpha = \frac{c_1[1-(\frac{T_{max}}{T_{min}})^{\frac{1}{4}}]}{c_2[1+(\frac{T_{max}}{T_{min}})^{\frac{1}{4}}]} \quad , \tag{7.3}$$

where

$$c_1 = (n+n_0)(n_1+n) \quad ,$$

$$c_2 = (n-n_0)(n_1-n) \quad .$$

By combining equations (7.1) and (7.3), we obtain

$$\frac{n^2}{c_1c_2} = \frac{\sqrt{T_{max}T_{min}}}{4n_0n_1(\sqrt{T_{min}}-\sqrt{T_{max}})} \quad . \tag{7.4}$$

The differential of the left side of the equation above is

$$\frac{d}{dn}(\frac{n^2}{c_1c_2})dn = \frac{ndn}{c_1c_2}\{2-\frac{n}{c_1}(n_1+n_0+2n)-\frac{n}{c_2}(n_1+n_0-2n)\} \tag{7.5}$$

and that of the right side is

$$d[\frac{\sqrt{T_{min}T_{max}}}{4n_0n_1(\sqrt{T_{min}}-\sqrt{T_{max}})}] = \frac{T_{min}dT_{max}}{8n_0n_1\sqrt{T_{max}}(\sqrt{T_{min}}-\sqrt{T_{max}})^2} - \frac{T_{max}dT_{min}}{8n_0n_1\sqrt{T_{min}}(\sqrt{T_{min}}-\sqrt{T_{max}})^2} \tag{7.6}$$

The relative error in n is determined by combining Eqs. (7.4), (7.5) and (7.6):

$$f(n)\frac{dn}{n} = \frac{dT_{min}}{T_{min}} \frac{1}{2} \frac{\sqrt{T_{max}}}{(\sqrt{T_{max}}-\sqrt{T_{min}})} - \frac{dTmax}{Tmax} \frac{1}{2} \frac{\sqrt{Tmin}}{(\sqrt{Tmax}-\sqrt{Tmin})} \quad (7.7)$$

with

$$f(n)=2[1- \frac{n(n_1+n_0)(n^2-n_0n_1)}{(n^2-n_0^2)(n_1^2-n^2)}] \quad (7.8)$$

The assumptions made here are:

1. That the error in n_1, the refractive indices of substrates, is comparatively insignificant.
2. That the errors for the two envelopes $T_{max}(\lambda)$ and $T_{min}(\lambda)$ are non-correlated

The relative error in n then is obtained

$$\frac{\Delta n}{n} = \frac{\Delta T}{T} \frac{1}{2}(\frac{\sqrt{Tmax}+\sqrt{Tmin}}{\sqrt{Tmax}-\sqrt{Tmin}}) \frac{1}{|f(n)|} \quad (7.9)$$

with $\Delta T/T$ being the relative precision of measurements ($\Delta T/T=\Delta T_{min}/T_{min} = \Delta T_{max}/T_{max}$).

The function $|f(n)|$ has been plotted on Fig.25 for $n_0=1$ and $n_1= 1.936$, corresponding to the typical values of refractive indices of garnet substrates in the infrared region. We can see that $|f(n)|$ is about 16 when n=2.1.

Similarly, from equation (5.27), we obtain

$$\frac{dt}{t} = d\lambda \frac{n(\lambda_1)\lambda_2^2-n(\lambda_2)\lambda_1^2}{\lambda_1\lambda_2(n(\lambda_1)\lambda_2-n(\lambda_2)\lambda_1)} + dn(\lambda_2)\frac{\lambda_1}{n(\lambda_1)\lambda_2-n(\lambda_2)\lambda_1} - dn(\lambda_1)\frac{\lambda_2}{n(\lambda_1)\lambda_2-n(\lambda_2)\lambda_1} \quad (7.10)$$

In the case of a weak dispersion, which is justified for bubble films, we have

$$n(\lambda_1) \cong n(\lambda_2) = n \quad , \qquad (7.11)$$

$$dn(\lambda_1) \cong dn(\lambda_2) = dn \quad .$$

This leads to

$$\frac{dt}{t} \cong d\lambda \frac{\lambda_2+\lambda_1}{\lambda_1\lambda_2} + \frac{dn}{n}\frac{\lambda_1}{\lambda_2-\lambda_1} - \frac{dn}{n}\frac{\lambda_2}{\lambda_2-\lambda_1} \quad . \qquad (7.12)$$

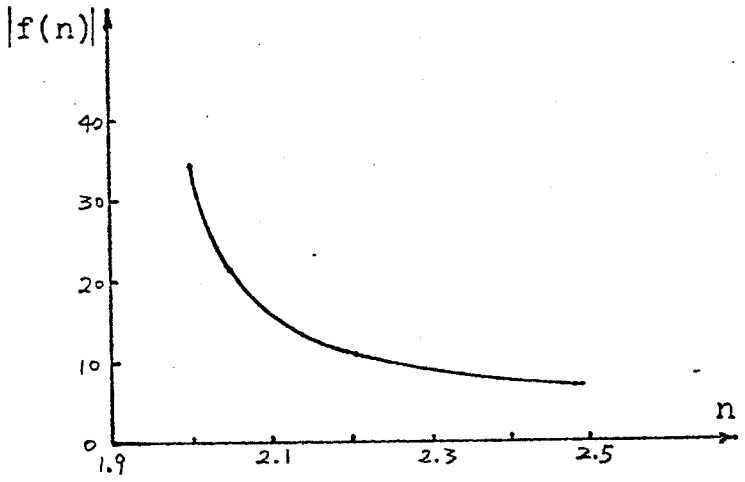

Fig.25 Typical values of $|f(n)|$ when $n_0=1$ and $n_1=1.936$.

The relative error in thickness can be expressed as

$$\frac{\Delta t}{t} \cong \Delta\lambda \frac{\lambda_2+\lambda_1}{\lambda_1\lambda_2} + \frac{\Delta n}{n}\frac{\lambda_1+\lambda_2}{\lambda_2-\lambda_1} \quad . \qquad (7.13)$$

Typically, with $\Delta T/T \simeq 1\%$, $\frac{\lambda_1+\lambda_2}{\lambda_2-\lambda_1} \simeq 4$ and $\Delta\lambda \frac{\lambda_2+\lambda_1}{\lambda_2-\lambda_1} \simeq 1\%$, we obtained

$$\frac{\Delta n}{n} \cong 1\ \% \qquad (7.14)$$

and

$$\frac{\Delta t}{t} \cong 5\ \% \qquad (7.15)$$

7.3 CONCLUSION

The purpose of this work is to demonstrate a way to verify the validity of the theories of the stripe domain wall stability in the cases when the magnetic field H is applied along or perpendicular to the easy direction of (111) bubble garnet films, respectively. By making use of two stability conditions, the magnetic thickness of the films was obtained wholly magnetically, and was compared with that from an independent optical measurement. In view of the fact that many measurements were involved to provide the necessary information about the film, it might be reasonable to think that the discrepancy would be large compared with the optical result, since the method itself has a drawback of amplifying the measurement errors when $H_{\pi}^{*}/(2Ku/Ms-4\pi Ms)$ is in a certain region. In fact, however, the actually observed discrepancies were not as large as expected. One reason is that, for samples under test, the value of $H_{\pi}^{*}/(2Ku/Ms-4\pi Ms)$ is not in this bad region. Another probable reason is the partial cancellation of errors from different measurments. Our work has shown that, if we treated the stability problem of the stripe domains in an in-plane magnetic field in the way Druyvesteyn et al. [2] did, we would obtain the magnetic thickness which deviates systematically from the

optical one very much. This deviation could not be caused by the experimental errors in magnetic parameters such as $H_{//}^{*}$, χ_o, etc., since a reasonable estimation had shown that, at the maximum, all these errors could produce a deviation only about one third of the deviation we actually obtained. Also, these errors could not produce systematic shifts for many samples. This systematic deviation was compensated by introducing the cubic anisotropy and the demagnetizing energy in the domain wall energy. From our work, it may be concluded that both cubic anisotropy and demagnetizing energies must be included in the total energy term, and in the domain wall energy term when the domain instability is concerned, in the case of a magnetic field applied in the film plane. Kooy's theory [1] is good enough for the domain instability problem in the case of magnetic field applied perpendicular to the film plane. Also, our work has shown that $H_{//}^{*}$ is not equal to 2Ku/Ms, the same conclusion that Druyvesteyn et al. [2] arrived at. A by-product of the present work is that it has shown that the film thickness can be obtained magnetically, so all other static magnetic parameters can be obtained magnetically without any optical measurement. It provides a possible way to measure the thickness of opaque magnetic bubble films if the optical method is not available.

Appendix A

DOMAIN WALL ENERGY

When an in-plane magnetic field $H_{//}$ is applied, the magnetization of the bubble film will make an angle θ_0 with the field direction which is chosen as the x-direction in the following calculation. For simplicity, a model of Bloch wall will be used [12].

When the spin magnetic moments of the adjacent atoms i and j makes an angle ϕ_{ij}, the exchange energy between the two moments is conveniently expressed in the form

$$w_{ij} = -2JS^2\cos\phi_{ij} \qquad \text{(A1.1)}$$

where J is the exchange integral and S the total spin quantum number of each atom. Eq. (A1.1) can be simplified as, for the small angle ϕ_{ij},

$$w_{ij} = JS^2\phi_{ij}^2+\text{const.} \qquad \text{(A1.2)}$$

Now let us set the z axis normal to the plane of the domain wall and its origin at the midpoint of the wall thickness, see Fig.26 . All spins are assumed to rotate in the X-Y plane. The angle θ of the spin orientation at z, as measured from the spin direction at z=0, changes from $-\theta_0$ at

$z=-z_0$ to $+\theta_0$ at $z=z_0$. The angle between neighboring spins is given by $(\frac{\partial\theta}{\partial z})a$, where a is the lattice constant. For a simple cubic lattice, the number of atoms per unit volume is $1/a^3$. It is convenient to set the constant in (A1.2) to zero and replace ϕ_{ij} by $(\frac{\partial\theta}{\partial z})a$, so we get the expression for the total exchange energy stored in the wall

$$\sigma_{ex}=\frac{JS^2}{a}\int_{-z_0}^{+z_0}(\frac{\partial\theta}{\partial z})^2dz \qquad \text{(A1.3)}$$

per unit area of the wall surface.

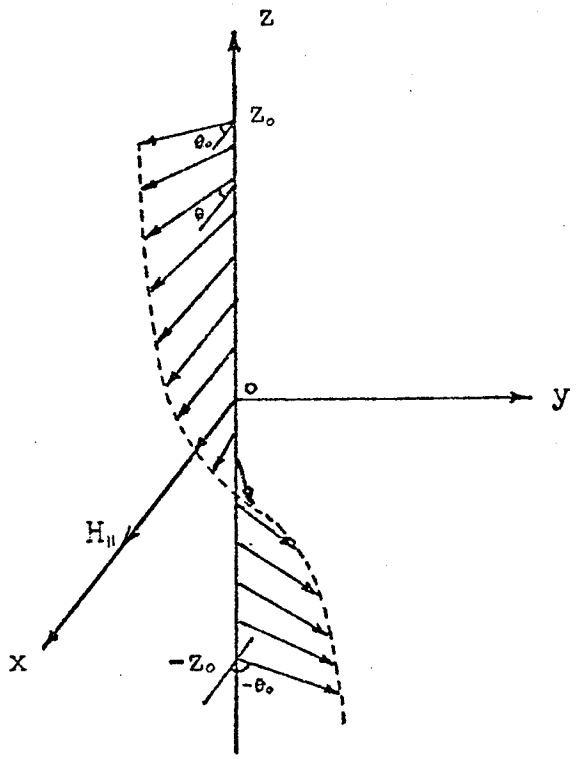

Fig.26 The angle of spin rotation

Eq.(A1.3) can be written in the general form

$$\sigma_{ex} = A \int_{-z_0}^{+z_0} \left(\frac{\partial\theta}{\partial z}\right)^2 dz \qquad \text{(A1.4)}$$

where A is the exchange coefficient which varies with different lattice structure.

On the other hand, the energy difference due to the magnetization in the wall in the field $H_{//}$ can be written as

$$\sigma_H = - \int_{-z_0}^{+z_0} MsH_{//}(\cos\theta - \cos\theta_0)\, dz \qquad \text{(A1.5)}$$

per unit area, since at equilibrium, the magnetization makes an angle θ_0 with field $H_{//}$.

In a similar way, if we express the energy terms other than those two mentioned previously as $g(\theta)$ per unit volume, we find the energy difference per unit area of the wall

$$\sigma_a = \int_{-z_0}^{+z_0} [g(\theta) - g(\theta_0)]\, dz \qquad \text{(A1.6)}$$

Thus the total wall energy per unit area is given by

$$\sigma = \sigma_{ex} + \sigma_a + \sigma_H = \int_{-z_0}^{+z_0} [g(\theta) - g(\theta_0) + A\left(\frac{\partial\theta}{\partial z}\right)^2 - MsH_{//}\cos\theta + MsH_{//}\cos\theta_0]\, dz \qquad \text{(A1.7)}$$

Now the state spin configuration can be obtained by minimizing the total energy (A1.7) for a small variation of the spin arrangement inside the wall. When the angle θ of the spin at z is changed by $\delta\theta$, the total energy of the wall is changed by

$$\delta\sigma = \int_{-z_0}^{+z_0} [\frac{\partial g(\theta)}{\partial \theta}\delta\theta + MsH \sin\theta\delta\theta + 2A(\frac{\partial\theta}{\partial z})(\frac{\partial\delta\theta}{\partial z})]\, dz \qquad (A1.8)$$

which should vanish for the stable spin arrangement. The last term of the integrand is treated by integrating by parts,

$$\int_{-z_0}^{+z_0} 2A(\frac{\partial\theta}{\partial z})(\frac{\partial\delta\theta}{\partial z})dz = 2A(\frac{\partial\theta}{\partial z})\delta\theta\Big|_{-z_0}^{+z_0} - \int_{-z_0}^{+z_0} 2A(\frac{\partial^2\theta}{\partial z^2})\delta\theta dz$$

$$= -\int_{-z_0}^{+z_0} 2A(\frac{\partial^2\theta}{\partial z^2})\delta\theta dz \qquad (A1.9)$$

because $(\frac{\partial\theta}{\partial z})=0$ at $z=\pm z_0$.

Then Eq. (A1.8) can be set to zero in such a way that

$$\int_{-z_0}^{+z_0} [\frac{\partial g(\theta)}{\partial\theta} + MsH_{//}\sin\theta - 2A(\frac{\partial^2\theta}{\partial z^2})]\delta\theta\, dz = 0 \qquad (A1.10)$$

In order that this condition be satisfied for any selection of $\delta\theta(z)$, the integrand must be zero, so we obtain the Euler equation

$$2A(\frac{\partial^2\theta}{\partial z^2}) = \frac{\partial g(\theta)}{\partial\theta} + MsH \sin\theta \qquad (A1.11)$$

Multiplying (A1.11) by $\frac{\partial\theta}{\partial z}$ on both sides and integrating it from $z=-z_0$ to $z=+z_0$, we get another relation

$$\frac{\partial\theta}{\partial z} = [\frac{g(\theta)-g(\theta_0)-MsH_{//}\cos\theta+MsH_{//}\cos\theta_0}{A}]^{\frac{1}{2}} \qquad (A.12)$$

From (A1.12) dz can be expressed in term of $d\theta$ as

$$dz=\frac{\sqrt{A}}{[g(\theta)-g(\theta_0)-MsH_{//}\cos\theta+MsH_{//}\cos\theta_0]^{\frac{1}{2}}}\,d\theta \qquad (A1.13)$$

By making use of both (A1.12) and (A1.13), we obtain the wall energy per unit area

$$\sigma=2\sqrt{A}\int_{-\theta_0}^{+\theta_0}[g(\theta)-g(\theta_0)-MsH_{//}\cos\theta+MsH_{//}\cos\theta_0]^{\frac{1}{2}}\,d\theta \qquad (A1.14)$$

Appendix B

ENERGY DERIVATIVES WITH RESPECT TO θ_o AND D/T

Derivatives of the total energy per unit volume with respect to θ_o and D/t are the following:

$$\frac{1}{4\pi M_S^2}\left(\frac{\partial E}{\partial \theta_o}\right) = \frac{2}{4\pi M_S^2 D}\frac{\partial \sigma}{\partial \theta_o} - \frac{Ku}{4\pi M_S^2}\sin 2\theta_o + \frac{H_{//}}{4\pi M_S}\sin\theta_o +$$

$$+ \frac{2}{3}\frac{K_1}{4\pi M_S^2}\sin^2\theta_o \sin 2\theta_o - \frac{1}{2}\frac{K_1}{4\pi M_S^2}\sin 2\theta_o \cos^2\theta_o +$$

$$+ \sin 2\theta_o \frac{4}{\pi^3(1+\sqrt{\mu})}\left(\frac{D}{t}\right)\sum_{n=odd}^{\infty}\frac{1}{n^3}\left(1-e^{-2n\pi\sqrt{\mu}\frac{t}{D}}\right) \qquad \text{(A2.1)}$$

$$\frac{1}{4\pi M_S^2}\left(\frac{\partial E}{\partial (D/t)}\right) = \frac{2}{4\pi M_S^2 D}\frac{\partial \sigma}{\partial (D/t)} - \frac{2t}{4\pi M_S^2 D^2}\sigma +$$

$$+ \frac{4\sin^2\theta_o}{\pi^3(1+\sqrt{\mu})}\sum_{n=odd}^{\infty}\frac{1}{n^3}\left(1-e^{-2n\pi\sqrt{\mu}\frac{t}{D}}\right) -$$

$$- \frac{8\sqrt{\mu}}{\pi^2(1+\sqrt{\mu})}\sin^2\theta_o \frac{t}{D}\sum_{n=odd}^{\infty}\frac{1}{n^2}e^{-2n\pi\sqrt{\mu}\frac{t}{D}} \qquad \text{(A2.2)}$$

$$\frac{1}{(4\pi M_S^2)^2}\left[\frac{\partial^2 E}{\partial\theta_o^2}\,\frac{\partial^2 E}{\partial(D/t)^2}-\left(\frac{\partial^2 E}{\partial\theta_o\partial(D/t)}\right)^2\right]=\left\{\frac{2}{4\pi M_S^2 D}\,\frac{\partial^2\sigma}{\partial\theta_o^2}-\frac{2Ku}{4\pi M_S^2}\cos2\theta_o+\right.$$

$$+\frac{H_{//}}{4\pi M_S}\cos\theta_o+\frac{K_1}{4\pi M_S^2}\left[\frac{4}{3}\sin^2\theta_o\cos2\theta_o-\cos2\theta_o\cos^2\theta_o+\frac{7}{6}\sin^2 2\theta_o\right]+$$

$$\left.+\cos2\theta_o\frac{8}{\pi^3(1+\sqrt{\mu})}\left(\frac{D}{t}\right)\sum_{n=odd}^{\infty}\frac{1}{n^3}\left(1-e^{-2n\pi\sqrt{\mu}\frac{t}{D}}\right)\right\}\cdot\left\{\frac{2}{4\pi M_S^2 D}\,\frac{\partial^2\sigma}{\partial(D/t)^2}-\right.$$

$$-\frac{4t}{4\pi M_S^2 D^2}\,\frac{\partial\sigma}{\partial(D/t)}+\frac{4t^2}{D^3}\,\frac{\sigma}{4\pi M_S^2}-\frac{16\mu}{\pi(1+\sqrt{\mu})}\sin^2\theta_o\left(\frac{t}{D}\right)^3\sum_{n=odd}^{\infty}\frac{1}{n}e^{-2n\pi\sqrt{\mu}\frac{t}{D}}\Big\}-$$

$$-\left\{\frac{2}{4\pi M_S^2 D}\,\frac{\partial^2\sigma}{\partial\theta_o\partial(D/t)}-\frac{2t}{4\pi M_S^2 D^2}\,\frac{\partial\sigma}{\partial\theta_o}+\frac{4\sin2\theta_o}{\pi^3(1+\sqrt{\mu})}\sum_{n=odd}^{\infty}\frac{1}{n^3}\left(1-e^{-2n\pi\sqrt{\mu}\frac{t}{D}}\right)-\right.$$

$$\left.-\frac{8\sqrt{\mu}}{\pi^2(1+\sqrt{\mu})}\sin2\theta_o\left(\frac{t}{D}\right)\sum_{n=odd}^{\infty}\frac{1}{n^2}e^{-2n\pi\sqrt{\mu}\frac{t}{D}}\right\}^2 \qquad \text{(A2.3)}$$

If the integration is replaced by summations by using Simpson's method, the derivatives of the domain wall energy with respect to θ_o and D/t can be expressed as,

$$\frac{1}{4\pi M_S^2 t}\,\frac{\partial\sigma}{\partial\theta_o}=\frac{\ell}{t}\,\frac{1}{6k}F_1(0)+\frac{\ell}{t}\,\frac{\theta_o}{12k}\,\frac{F_2(0)}{F_1(0)}+\frac{\ell}{t}\,\frac{2}{3k}\sum_{J=1}^{k}F_1(2J-1)+$$

$$+\frac{\ell}{t}\,\frac{\theta_o}{3k}\sum_{J=1}^{k}\frac{F_2(2J-1)}{F_1(2J-1)}+\frac{\ell}{t}\,\frac{1}{3k}\sum_{J=1}^{k-1}F_1(2J)+\frac{\ell}{t}\,\frac{\theta_o}{6k}\sum_{J=1}^{k-1}\frac{F_2(2J)}{F_1(2J)} \qquad \text{(A2.4)}$$

$$\frac{1}{4\pi M_S^2 t}\frac{\partial^2\sigma}{\partial\theta_o^2} = \frac{\ell}{t}\frac{1}{6k}\frac{F_2(0)}{F_1(0)} + \frac{\ell}{t}\frac{\theta_o}{12k}\frac{F_3(0)}{F_1(0)} - \frac{\ell}{t}\frac{\theta_o}{24k}\frac{F_2^2(0)}{F_1^3(0)} +$$

$$+ \frac{\ell}{t}\frac{2}{3k}\sum_{J=1}^{k}\frac{F_2(2J-1)}{F_1(2J-1)} + \frac{\ell}{t}\frac{\theta_o}{3k}\sum_{J=1}^{k}\frac{F_3(2J-1)}{F_1(2J-1)} - \frac{\ell}{t}\frac{\theta_o}{6k}\sum_{J=1}^{k}\frac{F_2^2(2J-1)}{F_1^3(2J-1)} +$$

$$+ \frac{\ell}{t}\frac{1}{3k}\sum_{J=1}^{k-1}\frac{F_2(2J)}{F_1(2J)} + \frac{\ell}{t}\frac{\theta_o}{6k}\sum_{J=1}^{k-1}\frac{F_3(2J)}{F_1(2J)} - \frac{\ell}{t}\frac{\theta_o}{12k}\sum_{J=1}^{k-1}\frac{F_2^2(2J)}{F_1^3(2J)} \qquad \text{(A2.5)}$$

$$\frac{1}{4\pi M_S^2 t}\frac{\partial\sigma}{\partial(D/t)} = \frac{\ell}{t}\frac{\theta_o}{12k}\frac{F_4(0)}{F_1(0)} + \frac{\ell}{t}\frac{\theta_o}{3k}\sum_{J=1}^{k}\frac{F_4(2J-1)}{F_1(2J-1)} + \frac{\ell}{t}\frac{\theta_o}{6k}\sum_{J=1}^{k-1}\frac{F_4(2J)}{F_1(2J)}$$

$$\text{(A2.6)}$$

$$\frac{1}{4\pi M_S^2 t}\frac{\partial^2\sigma}{\partial(D/t)^2} = \frac{\ell}{t}\frac{\theta_o}{12k}\frac{F_5(0)}{F_1(0)} - \frac{\ell}{t}\frac{\theta_o}{24k}\frac{F_4^2(0)}{F_1^3(0)} + \frac{\ell}{t}\frac{\theta_o}{3k}\sum_{J=1}^{k}\frac{F_5(2J-1)}{F_1(2J-1)} -$$

$$- \frac{\ell}{t}\frac{\theta_o}{6k}\sum_{J=1}^{k}\frac{F_4^2(2J-1)}{F_1^3(2J-1)} + \frac{\ell}{t}\frac{\theta_o}{6k}\sum_{J=1}^{k-1}\frac{F_5(2J)}{F_1(2J)} - \frac{\ell}{t}\frac{\theta_o}{12k}\sum_{J=1}^{k-1}\frac{F_4^2(2J)}{F_1^3(2J)} \qquad \text{(A2.7)}$$

$$\frac{1}{4\pi M_s^2 t}\frac{\partial^2\sigma}{\partial\theta_o\partial(D/t)} = \frac{\ell}{t}\frac{1}{12k}\frac{F_6(0)}{F_1(0)} - \frac{\ell}{t}\frac{\theta_o}{24k}\frac{F_2(0)F_4(0)}{F_1^3(0)} +$$

$$+ \frac{\ell}{t}\frac{1}{3k}\sum_{J=1}^{k}\frac{F_6(2J-1)}{F_1(2J-1)} - \frac{\ell}{t}\frac{\theta_o}{6k}\sum_{J=1}^{k}\frac{F_2(2J-1)F_4(2J-1)}{F_1^3(2J-1)} +$$

$$+ \frac{\ell}{t}\frac{1}{6k}\sum_{J=1}^{k-1}\frac{F_6(2J)}{F_1(2J)} - \frac{\ell}{t}\frac{\theta_o}{12k}\sum_{J=1}^{k-1}\frac{F_2(2J)F_4(2J)}{F_1^3(2J)} \qquad \text{(A2.8)}$$

where

$$F_1(JJ) = \{\cos^2(JJ\frac{\theta_o}{2k})-\cos^2\theta_o + \frac{abr}{2(a+b)}[\cos^4(JJ\frac{\theta_o}{2k})-\cos^4\theta_o] +$$

$$+ \frac{2}{3}\frac{abr}{a+b}[\sin^4(JJ\frac{\theta_o}{2k})-\sin^4\theta_o] - 2\frac{ab}{a+b}[\cos(JJ\frac{\theta_o}{2k})-\cos\theta_o] +$$

$$+[\sin^2(JJ\frac{\theta_o}{2k})-\sin^2\theta_o]\frac{8}{\pi^3(1+\sqrt{1+\frac{b}{a+b}})}\frac{b}{a+b}\frac{D}{t}\sum_{n=odd}^{\infty}\frac{1}{n^3}(1-e^{-2n\pi\sqrt{1+\frac{b}{a+b}}\frac{t}{D}})\}^{1/2}$$

(A2.9)

$$F_2(JJ) = \sin2\theta_o - \frac{JJ}{2k}\sin(JJ\frac{\theta_o}{k}) + \frac{abr}{a+b}[\sin2\theta_o\cos^2\theta_o - \frac{JJ}{2k}\sin(JJ\frac{\theta_o}{k})\cos^2(JJ\frac{\theta_o}{2k})] +$$

$$+\frac{4}{3}\frac{abr}{a+b}[(\frac{JJ}{2k})\sin^2(JJ\frac{\theta_o}{2k})\sin(JJ\frac{\theta_o}{k})-\sin^2\theta_o\sin2\theta_o] - 2\frac{ab}{a+b}[\sin\theta_o - \frac{JJ}{2k}\sin(JJ\frac{\theta_o}{2k})] +$$

$$+[\frac{JJ}{2k}\sin(JJ\frac{\theta_o}{k})-\sin2\theta_o]\frac{8}{\pi^3(1+\sqrt{1+\frac{b}{a+b}})}\frac{b}{a+b}\frac{D}{t}\sum_{n=odd}^{\infty}\frac{1}{n^3}(1-e^{-2n\pi\sqrt{1+\frac{b}{a+b}}\frac{t}{D}})$$

(A2.10)

$$F_3(JJ) = 2\cos 2\theta_o - \frac{1}{2}\left(\frac{JJ}{k}\right)^2 \cos\left(JJ\frac{\theta_o}{k}\right) + 2\,\frac{abr}{a+b}\left[\cos 2\theta_o \cos^2\theta_o - \right.$$

$$-\left(\frac{JJ}{2k}\right)^2 \cos\left(JJ\frac{\theta_o}{k}\right)\cos^2\left(JJ\frac{\theta_o}{2k}\right) + \frac{1}{3}\left(\frac{JJ}{k}\right)^2 \sin^2\left(JJ\frac{\theta_o}{2k}\right)\cos\left(JJ\frac{\theta_o}{k}\right) - \frac{4}{3}\sin^2\theta_o \cos 2\theta_o\Big] -$$

$$-\frac{7}{3}\,\frac{abr}{a+b}\left[\sin^2 2\theta_o - \left(\frac{JJ}{2k}\right)^2 \sin^2\left(JJ\frac{\theta_o}{k}\right)\right] - \frac{2ab}{a+b}\left[\cos\theta_o - \left(\frac{JJ}{2k}\right)^2 \cos\left(JJ\frac{\theta_o}{2k}\right)\right] +$$

$$+\left[\left(\frac{JJ}{2k}\right)^2 \cos\left(JJ\frac{\theta_o}{k}\right) - \cos 2\theta_o\right] \frac{16}{\pi^3\left(1+\sqrt{1+\frac{b}{a+b}}\right)}\,\frac{b}{a+b}\,\frac{D}{t}\sum_{n=odd}^{\infty}\frac{1}{n^3}\left(1-e^{-2n\pi\sqrt{1+\frac{b}{a+b}}\,\frac{t}{D}}\right)$$

(A2.11)

$$F_4(JJ) = \left[\sin^2\left(JJ\frac{\theta_o}{2k}\right) - \sin^2\theta_o\right]\cdot\left\{\frac{8}{\pi^3\left(1+\sqrt{1+\frac{b}{a+b}}\right)}\,\frac{b}{a+b}\sum_{n=odd}^{\infty}\frac{1}{n^3}\left(1-e^{-2n\pi\sqrt{1+\frac{b}{a+b}}\,\frac{t}{D}}\right) -\right.$$

$$\left. -\frac{16\sqrt{1+\frac{b}{a+b}}}{\pi^2\left(1+\sqrt{1+\frac{b}{a+b}}\right)}\,\frac{b}{a+b}\,\frac{t}{D}\sum_{n=odd}^{\infty}\frac{1}{n^2}\,e^{-2n\pi\sqrt{1+\frac{b}{a+b}}\,\frac{t}{D}}\right\} \qquad \text{(A2.12)}$$

$$F_5(JJ) = \left[\sin^2\theta_o - \sin^2\left(JJ\frac{\theta_o}{2k}\right)\right]\cdot$$

$$\cdot\,\frac{32\left(1+\frac{b}{a+b}\right)}{\pi^2\left(1+\sqrt{1+\frac{b}{a+b}}\right)}\,\frac{b}{a+b}\left(\frac{t}{D}\right)^3\sum_{n=odd}^{\infty}\frac{1}{n}\,e^{-2n\pi\sqrt{1+\frac{b}{a+b}}\,\frac{t}{D}} \qquad \text{(A2.13)}$$

$$F_6(JJ) = \left\{\sin^2\left(JJ\frac{\theta_o}{2k}\right)-\sin^2\theta_o+\theta_o\left[\frac{JJ}{2k}\sin\left(JJ\frac{\theta_o}{k}\right)-\sin 2\theta_o\right]\right\}\cdot$$

$$\cdot\left\{\frac{8}{\pi^3\left(1+\sqrt{1+\frac{b}{a+b}}\right)}\frac{b}{a+b}\sum_{n=odd}^{\infty}\frac{1}{n^3}\left(1-e^{-2n\pi\sqrt{1+\frac{b}{a+b}}\,\frac{t}{D}}\right)-\right.$$

$$\left.-\frac{16\sqrt{1+\frac{b}{a+b}}}{\pi^2\left(1+\sqrt{1+\frac{b}{a+b}}\right)}\frac{b}{a+b}\frac{t}{D}\sum_{n=odd}^{\infty}\frac{1}{n^2}e^{-2n\pi\sqrt{1+\frac{b}{a+b}}\,\frac{t}{D}}\right\}. \qquad (A2.14)$$

with

$$a=\frac{H_{\parallel}}{4\pi M_S}$$

$$b=\frac{H_{\parallel}}{\frac{2Ku}{M_S}-4\pi M_S}$$

$$r=\frac{K_1}{M_S H_{\parallel}}$$

$$\ell=\frac{4\sqrt{AKu}}{4\pi M_S^2}$$

k is the number of divisions of θ_o and is an integer. JJ is a notation which will be replaced by 2J or 2J-1 in the sum over J.

Appendix C

SUMMARY OF THE THEORY OF KOOY AND ENZ

We shall now summarize the theory of stripe domains as developed by Kooy and Enz [1]. Consider a plate of thickness t, containing parallel stripes of alternating magnetization as shown in Fig.27 .

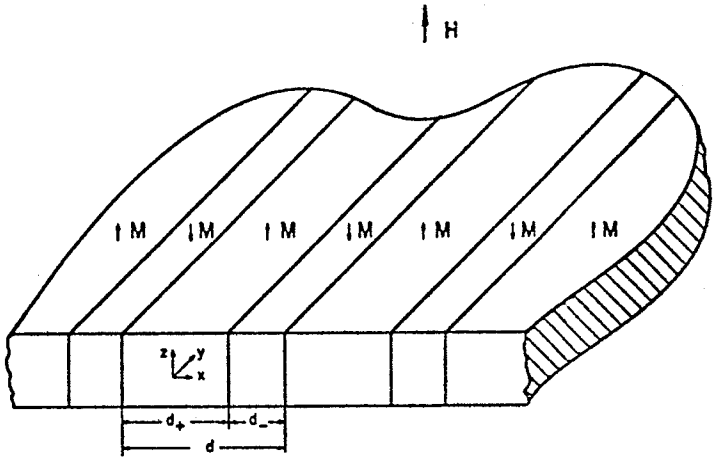

Fig.27 Stripe domains of alternating magnetization

If a field H is applied along z axis which is parallel to the preferential direction of the film magnetization as shown, then the domains magnetized parallel to H will increase in width to a value d_+ which is greater than d_-, the width that the antiparallel domains achieve. d_+ and d_- are

equal in the absence of an applied field. This model is unrealistic in a sense since in practice domains do not have straight walls but instead meander; however, as an approximation to the general case, this model gives considerable insight into the problem.

The wall energy per cm^2 of the plate is

$$E_w = 2t\sigma/D \qquad (A3.1)$$

The energy E per cm^2 of the plate in the applied field H is given by

$$\begin{aligned} E_H &= -HM_S t(d_+ - d_-)/D \\ &= -HM_S tM/M_S \end{aligned} \qquad (A3.2)$$

The magnetic charge density ρ_o on the surface is, according to the geometry of the problem,

$$\rho_o = M_S \frac{d_+ - d_-}{d_+ + d_-} + \frac{4}{\pi} M_S \sum_{n=1}^{\infty} \frac{1}{n} \sin\frac{n\pi d_+}{d_+ - d_-} \cos\frac{2\pi nx}{d_+ + d_-} \qquad (A3.3)$$

representing a square wave.

The potential in the plate due to this charge distribution can be expressed by Fourier series

$$V_i = b_o z + \sum_{n=1}^{\infty} b_n \sin\frac{n\pi d_+}{d_+ + d_-} \cos\frac{2\pi nx}{d_+ + d_-} \sinh\frac{2\pi nz\sqrt{\mu}}{d_+ + d_-} \qquad (A3.4)$$

with

$$b_o = 4\pi M_S \frac{d_+ - d_-}{d_+ + d_-} \qquad (A3.5)$$

and

$$b_n = \frac{8}{\pi} M_S (d_+ + d_-) \frac{1}{n^2} \left[\sinh\left(\frac{n\pi t\sqrt{\mu}}{d_+ + d_-}\right) + \sqrt{\mu} \cosh\left(\frac{n\pi t\sqrt{\mu}}{d_+ + d_-}\right)\right] \qquad (3.6)$$

The demagnetization energy per cm^2 of the plate can be calculated from the integration

$$E_D = \frac{1}{2(d_+ + d_-)} \int_{-\frac{1}{2}(d_+ + d_-)}^{+\frac{1}{2}(d_+ + d_-)} \rho_o V_i \, dx \qquad (A3.7)$$

which gives the expression for the demagnetization energy E_D, including the contribution of 'μ-effect' for $\mu \simeq 1$ ($\mu = 1 + 2\pi Ms^2/Ku$),

$$E_D = 2\pi M_S^2 t \left(\frac{M}{M_S}\right)^2 + \frac{16}{\pi^2} M_S^2 \frac{t\sqrt{\mu}}{\alpha} \sum_{n=1}^{\infty} \frac{1}{n^3} \sin^2\left[\frac{n\pi}{2}\left(1+\frac{M}{M_S}\right)\right] \frac{\sinh(n\pi\alpha)}{\sinh(n\pi\alpha)+\sqrt{\mu}\cosh(n\pi\alpha)} \qquad (A3.8)$$

where

$$M/M_S = (d_+ - d_-)/D$$

$$\alpha = t\sqrt{\mu}/D$$

The stable domain width d_+ and d_- in an arbitrary stage of magnetization can be found by equating the derivatives $\frac{\partial E}{\partial (M/M_S)}$ and $\frac{\partial E}{\partial \alpha}$ of the total energy $E = E_W + E_H + E_D$ to zero, giving the simultaneous equations

$$\frac{4\pi M - H}{4\pi M_S} + \frac{1}{\pi^2 \alpha} \sum_{n=1}^{\infty} \frac{1}{n^2} \sin\left[n\pi\left(1+\frac{M}{M_S}\right)\right]\left[1-\exp(-2\pi n\alpha)\right] = 0 \qquad (A3.9)$$

$$\frac{1}{4\pi^2\alpha^2} \sum_{n=1}^{\infty} \frac{1}{n^3} \sin^2\left[\frac{n\pi}{2}\left(1+\frac{M}{M_S}\right)\right]\left[1-(1+2\pi n\alpha)\exp(-2\pi n\alpha)\right] - \frac{\sigma}{(4M_S)^2 t} = 0 \qquad (A3.10)$$

in the case $\mu = 1$.

when H=0, M=0, Eq. (A3.7) will give normalized characteristic length as a function of normalized stripe period,

$$\frac{\ell}{t} = \frac{1}{\pi^3}\left(\frac{D}{t}\right)^2 \sum_{n=\text{odd}}^{\infty} \frac{1}{n^3}\left[1-\left(1+2n\pi\frac{t}{D}\right)\exp\left(-2n\pi\frac{t}{D}\right)\right] \qquad \text{(A3.11)}$$

By differentiating Eq. (A3.6), we obtain the initial susceptibility χ_0,

$$\frac{dM}{M_S} - \frac{dH}{4\pi M_S} + \frac{1}{\pi\alpha}\sum_{n=1}^{\infty} \frac{1}{n}\frac{1}{M_S}\cos\left[n\pi\left(1+\frac{M}{M_S}\right)\right]\left[1-\exp(-2\pi n\alpha)\right] dM=0 \qquad \text{(A3.12)}$$

$$\chi_o=\left(\frac{dM}{dH}\right)_{M=0} = \frac{1}{4\pi}\left[1+\frac{D}{\pi t}\sum_{n=1}^{\infty} \frac{1}{n}(-1)^n\left[1-\exp\left(-2\pi n\frac{t}{D}\right)\right]\right]^{-1} \qquad \text{(A3.13)}$$

Appendix D

ENERGY EXPRESSION IN FERROMAGNETIC RESONANCE

When a DC magnetic field is applied in the (110) plane for the (111) films, as is shown in Fig.15, the total free energy of the system, E, is the sum of Zeeman energy, demagnetization energy, uniaxial magnetic anisotropy energy and cubic magnetocrystalline anisotropy energy, if the contribution from K_2 is neglected.

Zeeman energy can be written as

$$\begin{aligned} E_Z &= -\vec{M}\cdot\vec{H} \\ &= -(M_S\sin\theta\cos\phi\vec{x}_o+M_S\sin\theta\sin\phi\vec{y}_o+M_S\cos\theta\vec{z}_o)\cdot(H\cos\beta\vec{z}_o+H\sin\beta\vec{x}_o) \\ &= -M_SH(\sin\theta\cos\phi\sin\beta+\cos\theta\cos\beta) \end{aligned} \qquad (A4.1)$$

Demagnetization energy is

$$\begin{aligned} E_D &= \frac{1}{2}(D_xM_x^2+D_yM_y^2+D_zM_z^2) \\ &= D_zM_z^2/2 \\ &= 2\pi M_S^2\cos^2\theta \end{aligned} \qquad (A4.2)$$

since $D_x=D_y=0$, $D_z=4\pi$ for the infinite plane.

The easy direction is [111] normal to the plane. This leads to the uniaxial anisotropy expressed as

$$E_u = Ku\sin^2\theta \qquad (A4.3)$$

The cubic anisotropy energy in general form [15] is

$$E_C = K_1(\alpha_1^2\alpha_2^2+\alpha_1^2\alpha_3^2+\alpha_2^2\alpha_3^2) \qquad (A4.4)$$

where α_1, α_2 and α_3 are cosines of $\vec{M}$ with three edges of cubic.

With the help of Fig.28, the unit vectors in frame (X,Y,Z) can be expressed by those in frame (X',Y',Z'). Here we have

$$\vec{z}_o = \frac{1}{\sqrt{3}}(\vec{x}'_o + \vec{y}'_o + \vec{z}'_o)$$

$$\vec{y}_o = \frac{1}{\sqrt{2}}(-\vec{x}'_o + \vec{y}'_o) \qquad (A4.5)$$

$$\vec{x}_o = \frac{1}{\sqrt{6}}(\vec{x}'_o + \vec{y}'_o - 2\vec{z}'_o)$$

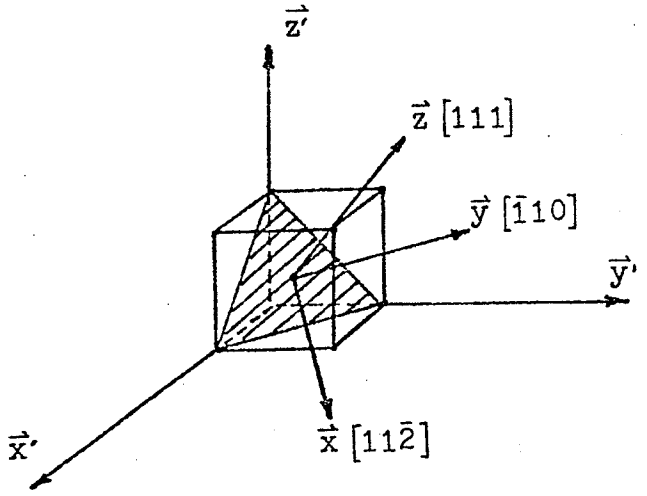

Fig.28 Coordinate system used to calculate α_1, α_2, α_3.

We will rewrite the magnetization in frame (X',Y',Z')

$$\vec{M} = M_S\sin\theta\cos\phi\vec{x}_o + M_S\sin\theta\sin\phi\vec{y}_o + M_S\cos\theta\vec{z}_o$$

$$= M_S\left[\frac{1}{\sqrt{6}}\sin\theta\cos\phi - \frac{1}{\sqrt{2}}\sin\theta\sin\phi + \frac{1}{\sqrt{3}}\cos\theta\right]\vec{x}_o +$$

$$+ M_S\left[\frac{1}{\sqrt{6}}\sin\theta\cos\phi + \frac{1}{\sqrt{2}}\sin\theta\sin\phi + \frac{1}{\sqrt{3}}\cos\theta\right]\vec{y}_o +$$

$$+ M_S\left[\frac{1}{\sqrt{3}}\cos\theta - \frac{2}{\sqrt{6}}\sin\theta\cos\phi\right]\vec{z}_o \qquad \text{(A4.6)}$$

$$\alpha_1 = \frac{1}{\sqrt{6}}\sin\theta\cos\phi - \frac{1}{\sqrt{2}}\sin\theta\sin\phi + \frac{1}{\sqrt{3}}\cos\theta$$

$$\alpha_2 = \frac{1}{\sqrt{6}}\sin\theta\cos\phi + \frac{1}{\sqrt{2}}\sin\theta\sin\phi + \frac{1}{\sqrt{3}}\cos\theta \qquad \text{(A4.7)}$$

$$\alpha_3 = -\frac{2}{\sqrt{6}}\sin\theta\cos\phi + \frac{1}{\sqrt{3}}\cos\theta$$

since

$$(\alpha_1\alpha_2)^2 + (\alpha_1\alpha_3)^2 + (\alpha_2\alpha_3)^2 = \frac{1}{2}\left[1 - (\alpha_1^4 + \alpha_2^4 + \alpha_3^4)\right]$$

We obtain the cubic anisotropy energy

$$E_c = K_1\left(\frac{1}{4}\sin^4\theta + \frac{1}{3}\cos^4\theta + \frac{\sqrt{2}}{3}\sin^3\theta\cos\theta\cos 3\phi\right) \qquad \text{(A4.8)}$$

When $\vec{M}$ is along <110> direction, $\cos(3\phi)=0$, so we obtain

$$E_c = K_1\left(\frac{1}{4}\sin^4\theta + \frac{1}{3}\cos^4\theta\right) \qquad \text{(A4.9)}$$

BIBLIOGRAPHY

[1] C.Kooy and U.Enz, Philips Res. Repts. 15, 7 (1960)

[2] W.F.Druyvesteyn, J.W.F.Dorleijn and P.J.Rijnierse, J.Appl.Phys. 44, 2397 (1973)

[3] Y.Shimada and H.Kojima, J.Appl.Phys. 44, 5125(1973)

[4] Mou-Hsin Yang and M.W.Muler, J.Appl.Phys. 45, 4130(1974)

[5] I.Maartense, C.W.Searle and M.G.Mier, J.Appl. Phys. 49, 1882 (1978)

[6] A.A.Thiele, J.Appl. Phys. 41, 1139 (1979)

[7] I.Maartense, J.Appl. Phys. 53, 2466 (1982)

[8] P.W.Shumate, Jr., J.Appl. Phys. 44, 3323 (1973)

[9] A.Hubert, A.P.Malozemoff, and J.C.Deluca, J.Appl.Phys. 45, 3562 (1974)

[10] For example, Debonte had discussed this problem in his paper. IEEE, Mag-11, 3 (1975)

[11] T.G.W.Blake, Ching-Cheng Shir, Yih-Otu and Edward Della Torre, IEEE, MAG-18, 985 (1982)

[12] S.Chikazumi, Physics of Magnetism (Wiley, New York, 1964), P.189

[13] J.H.E.Griffiths, Nature 158, 670 (1946)

[14] L.D.Landau and E.M.Lifshitz, Physik Z.Sowjet 8, 183 (1935)

[15] A.H.Morrish, "The physical principles of magnetism" (John Wiley and Sons, Inc. (1965))

[16] M.D.Sturge, R.C.Lecraw, R.D.Pierce, S.J.Licht and L.K.Shick, Phys. Rev. BI, 1070 (1973)

[17] Hiroshi Makino and Yasuharu Hidaka, Mat. Res. Bull., 16, 957 (1981)

[18] JC Manifacier, J Gasiot and JP Fillard, J. Phys. E 9(11) 1002, 1976 5R

[19] O.S. Heavens, Optical properties of thin solid films, P.63-65

[20] S.H.Wemple and W.J.Tabor, J.Appl. Phys. 44, 1395 (1973)